



RESEARCH

Open Access



Orally biomimetic metal-phenolic nanozyme with quadruple safeguards for intestinal homeostasis to ameliorate ulcerative colitis

Yuanyuan Zhu^{1,2†}, Xiaoling Huang^{3†}, Zhichao Deng⁴, Ting Bai⁵, Bowen Gao⁴, Chenxi Xu⁴, Junlong Fu⁴, Yuanru Zhao⁴, Yujie Zhang⁴, Mingxin Zhang⁶, Mingzhen Zhang^{4,7*} , Mei Yang^{1*}  and Lina Chen^{2,7*} 

Abstract

Background Ulcerative colitis (UC) is defined by persistent inflammatory processes within the gastrointestinal tract of uncertain etiology. Current therapeutic approaches are limited in their ability to address oxidative stress, inflammation, barrier function restoration, and modulation of gut microbiota in a coordinated manner to maintain intestinal homeostasis.

Results This study involves the construction of a metal-phenolic nanozyme (Cur-Fe) through a ferric ion-mediated oxidative coupling of curcumin. Cur-Fe nanozyme exhibits superoxide dismutase (SOD)-like and $\cdot\text{OH}$ scavenging activities, demonstrating significant anti-inflammatory and anti-oxidant properties for maintaining intracellular redox balance in vitro. Drawing inspiration from *Escherichia coli* Nissle 1917 (EcN), a biomimetic Cur-Fe nanozyme (CF@EM) is subsequently developed by integrating Cur-Fe into the EcN membrane (EM) to improve the in vivo targeting ability and therapeutic effectiveness of the Cur-Fe nanozyme. When orally administered, CF@EM demonstrates a strong ability to colonize the inflamed colon and restore intestinal redox balance and barrier function in DSS-induced colitis models. Importantly, CF@EM influences the gut microbiome towards a beneficial state by enhancing bacterial diversity and shifting the compositional structure toward an anti-inflammatory phenotype. Furthermore, analysis of intestinal microbial metabolites supports the notion that the therapeutic efficacy of CF@EM is closely associated with bile acid metabolism.

Conclusion Inspired by gut microbes, we have successfully synthesized a biomimetic Cur-Fe nanozyme with the ability to inhibit inflammation and restore intestinal homeostasis. Collectively, without appreciable systemic toxicity, this work provides an unprecedented opportunity for targeted oral nanomedicine in the treatment of ulcerative colitis.

[†]Yuanyuan Zhu and Xiaoling Huang contributed equally to this work.

*Correspondence:

Mingzhen Zhang
mzhang21@xjtu.edu.cn
Mei Yang
meiyang@xjtu.edu.cn
Lina Chen
chenlin@xjtu.edu.cn

Full list of author information is available at the end of the article



© The Author(s) 2024. **Open Access** This article is licensed under a Creative Commons Attribution-NonCommercial-NoDerivatives 4.0 International License, which permits any non-commercial use, sharing, distribution and reproduction in any medium or format, as long as you give appropriate credit to the original author(s) and the source, provide a link to the Creative Commons licence, and indicate if you modified the licensed material. You do not have permission under this licence to share adapted material derived from this article or parts of it. The images or other third party material in this article are included in the article's Creative Commons licence, unless indicated otherwise in a credit line to the material. If material is not included in the article's Creative Commons licence and your intended use is not permitted by statutory regulation or exceeds the permitted use, you will need to obtain permission directly from the copyright holder. To view a copy of this licence, visit <http://creativecommons.org/licenses/by-nc-nd/4.0/>.

Keywords Metal-phenolic nanozyme, Ulcerative colitis, Oxidative stress, Inflammation, Intestinal homeostasis

Introduction

Ulcerative colitis (UC) is a non-specific inflammatory bowel disease that affects the colon and rectum, characterized by continuous and diffuse inflammation and ulceration of the mucosal lining [1]. The prevalence of UC is rapidly increasing with social progress, becoming a global disease [2, 3]. The pathogenesis of UC is currently unclear. The most widely accepted hypothesis is that a combination of factors, such as genetic predisposition [4], abnormal immune regulation [5–7], changes in the intestinal microbiota [8, 9], and external environmental stimuli [10, 11], contribute to a dysregulation of intestinal homeostasis, which in turn triggers inflammatory bowel disease. Currently, various therapeutic strategies are used in clinical practice to alleviate clinical symptoms based on the progression of UC. However, the high cost of treatment and potential toxic side effects limit their long-term use [12]. Moreover, relying on a single therapeutic modality often does not yield optimal clinical outcomes [13]. Therefore, synergistic treatment with multiple interventions holds great promise for improving clinical outcomes.

Curcumin, a natural polyphenolic compound, is widely acknowledged for its inherent anti-inflammatory and antioxidant properties, it is extensively utilized in the food industry owing to its excellent biocompatibility [14, 15]. However, its limited water solubility and low bioavailability hinder its application in inflammatory diseases [16]. The unique chemical structure of polyphenolic active compounds enables them to form complexes with metal ions, thereby enhancing their water solubility, while metal-phenolic interactions exhibit catalytic properties [17, 18]. Compared with the disadvantages of high price and poor stability of natural enzymes, nanozymes, as a kind of nanomaterials with enzyme-like properties, have been widely researched and applied due to their many unique advantages [19], such as low cost, high stability, easy modification, and tunable catalytic activity [20, 21]. Among them, antioxidant nanozymes can effectively alleviate oxidative stress and inhibit inflammatory responses, exhibiting promising therapeutic effects in the treatment of ulcerative colitis [22, 23].

The anaerobic environment of the colon makes it the region with the highest bacterial density and diversity in the intestinal tract [24]. Oxidative stress, caused by an imbalance between reactive oxygen species (ROS) and antioxidant defense mechanisms, has been implicated in the pathogenesis of UC [25]. Excessive ROS production can lead to damage to the intestinal epithelial barrier, promoting inflammation and exacerbating the symptoms of UC [26, 27]. The gut microbiota, as an important

component of intestinal microecology, may contribute to potential alterations in disease states due to dramatic changes in its structure and function. Remodeling the composition of the gut microbiota and restoring the normal metabolic function of the microbiota are the current therapeutic goals of probiotic agents [28–30]. As a probiotic, *Escherichia coli* Nissle 1917 (EcN) is widely used in the treatment of inflammatory bowel disease due to its excellent antibacterial, anti-inflammatory, and gut microbiota-regulating properties [31].

Here, we have successfully synthesized a Cur-Fe nanozyme with anti-inflammatory and antioxidant properties by complexing ferric ions with curcumin. Through in vitro and in vivo experiments, we found that the Cur-Fe nanozyme could alleviate the oxidative stress at inflammation sites by scavenging ROS, while simultaneously reducing the inflammatory response by down-regulating the expression of pro-inflammatory cytokines and inhibiting the transformation of M1 macrophages. To enhance the concentration of Cur-Fe nanozyme at inflammation sites and prolong its therapeutic duration, we integrated *Escherichia coli* Nissle 1917 membrane (EM) with Cur-Fe nanozyme to create a biomimetic nanozyme CF@EM. The anti-inflammatory and antioxidant effects of CF@EM were further augmented by the intestinal colonization of EM, leading to an increase in the abundance of the beneficial bacterial genera such as *Lactobacillus* and *Muribaculum*, and a decrease in the pathogenic genera *Clostridium-sensu-stricto* and *Escherichia-Shigella*. Additionally, CF@EM regulated various active metabolites, including secondary bile acids, to synergistically maintain the balance of intestinal microbiota composition and restore normal levels of intestinal metabolites, thereby achieving multi-targeted combination therapy. This strategy holds broad clinical application prospects in the prevention and treatment of UC (see Fig 1).

Materials and methods

Materials

Curcumin, $\text{FeCl}_3 \cdot 6\text{H}_2\text{O}$, and polyvinylpyrrolidone were purchased from Shanghai Macklin Biochemical Technology Co., Ltd (Shanghai, China). Triton X-100, TMB, MTT, and LPS (from *Escherichia coli* O55:B5) were purchased from Beijing Solarbio Science & Technology Co., Ltd (Beijing, China). *Escherichia coli* Nissle 1917 was purchased from the BeNa Culture Collection (Beijing, China). The fluorescent dye DiR was purchased from Promokine (Heidelberg, Germany). ABTS, DCFH-DA, and DHE were purchased from Beyotime Biotechnology (Shanghai, China). Calcein-AM/PI and Annexin V-FITC/PI apoptosis kits were purchased from Elabscience

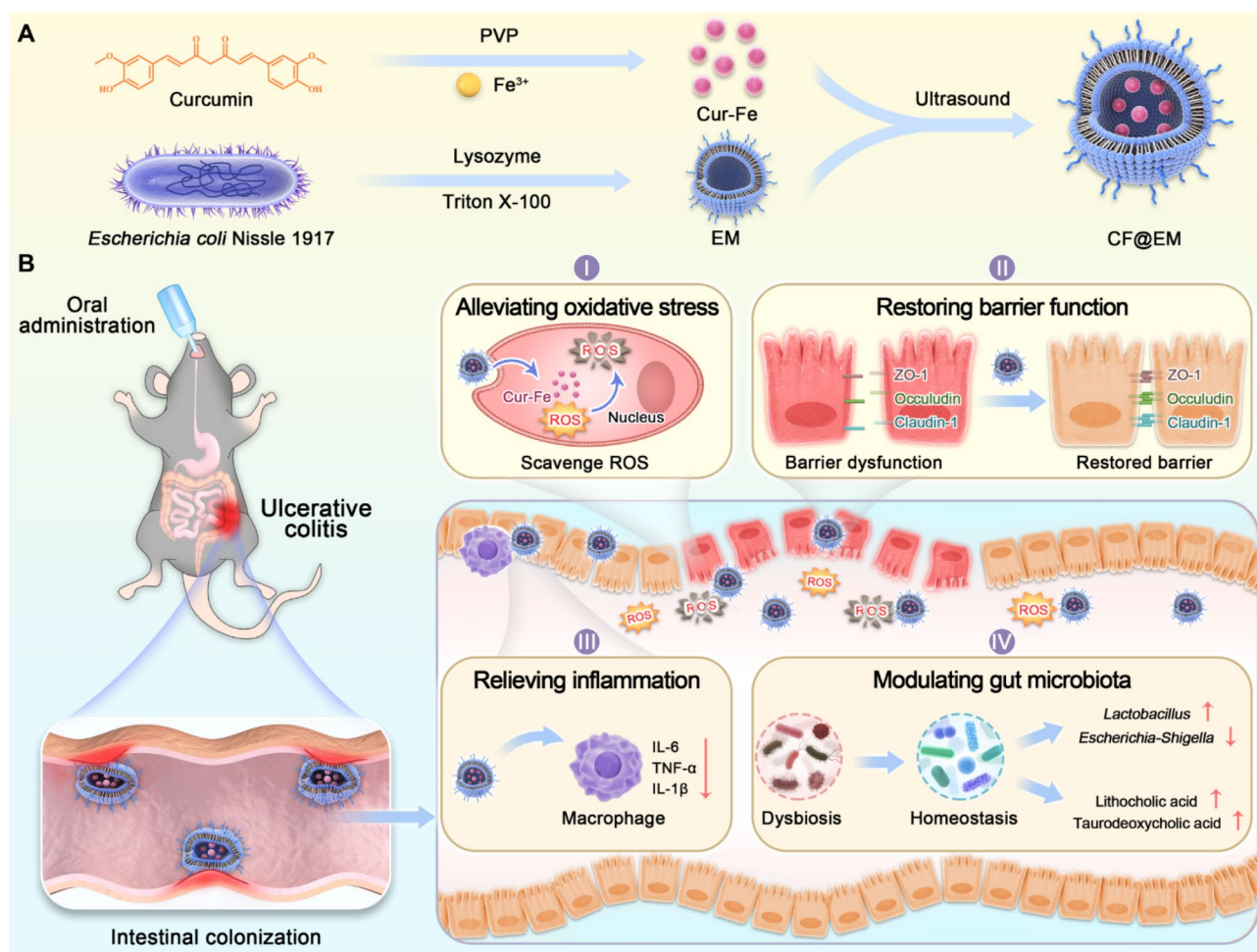


Fig. 1 Schematic illustration showing the synthesis and action mechanisms of biomimetic Cur-Fe nanozyme against ulcerative colitis. **(A)** Preparation of biomimetic Cur-Fe nanozyme (CF@EM) inspired by the probiotic membrane. **(B)** The intestinal colonization capacity of the probiotic membrane increases the concentration and duration of action of CF@EM at the site of inflammation, synergistically alleviating oxidative stress, restoring intestinal barrier function, relieving inflammation, and modulating the gut microbiota to alleviate ulcerative colitis

Biotechnology Co., Ltd (Wuhan, China). SOD assay kit-WST was purchased from Dojindo (Shanghai, China). MPO assay kit was purchased from the Nanjing Jian-jian Bioengineering Research Institute (Nanjing, China). DSS was purchased from MP Biomedicals (Santa Ana, CA, USA). APC rat anti-mouse CD86 (561964) was purchased from Becton, Dickinson, and Company (Franklin Lakes, NJ). Anti-claudin-1 antibody (13050-1-AP), anti-ZO-1 antibody (CL488-21773), and anti-occludin antibody (CL594-13409) were purchased from Proteintech (Wuhan, China).

Preparation of Cur-Fe and CF@EM

66 mg of polyvinylpyrrolidone (PVP) was dissolved in 5 mL of methanol, then 20 mg of $\text{FeCl}_3 \cdot 6\text{H}_2\text{O}$ was dissolved in 1 mL of methanol and added dropwise to the PVP solution with stirring. After 5 min, 10 mg of curcumin dissolved in 1 mL of methanol was added dropwise with

stirring for 3 h. Finally, the product was dialyzed against water overnight to obtain Cur-Fe.

EcN bacteria were grown in LB medium and shaken overnight at 37 °C at 180 rpm. 400 μL of EcN suspension was then added to 400 mL of fresh LB medium until an optical density of 1.0 at 600 nm was reached. Bacteria were isolated by centrifugation at 3000 g for 20 min at 4 °C and then resuspended in 40 mL buffer containing 1.5 M pH 8.0 Tris-HCl, 20 mM sucrose, 400 $\mu\text{g}/\text{mL}$ lysozyme, and 0.2 mM EDTA. After 20 min, 10 $\mu\text{g}/\text{mL}$ aprotinin, 1 mM PMSE, and the same volume of extraction buffer (50 mM pH 7.4 Tris-HCl, 2% Triton X-100, 10 $\mu\text{g}/\text{mL}$ DNase, and 10 mM MgCl_2) were added. After 30 min of incubation on ice, the samples were centrifuged at 5000 g for 5 min. The supernatant was then centrifuged at 17,000 g for 20 min at 4 °C, and the precipitated membrane fraction was washed twice to obtain EM. CF@EM was synthesized under ultrasound by mixing EMs with Cur-Fe nanozymes at a concentration ratio of 1:1.

Characterization of Cur-Fe and CF@EM

The morphological characteristics of Cur-Fe and CF@EM were observed by TEM. 10 μL of Cur-Fe or CF@EM solution was taken and dropped on a copper grid for TEM. Then samples were dried and used for TEM observation. Particle size and zeta potential of Cur-Fe and CF@EM were measured by DLS. Cur-Fe and CF@EM were dispersed in 1 mL of ultrapure water and measured 3 times for each sample using a Malvern particle size analyzer. CF@EM was also characterized by the Coomassie brilliant blue method. The volumes of sample and up-sampling buffer were calculated based on the protein concentration of the samples. At the end of electrophoresis, the gels were transferred to a Coomassie brilliant blue solution and incubated on a horizontal shaker for 1 h. The gel was then destained with the destaining solution until the gel was destained and the protein bands were visible.

ROS scavenging evaluation of Cur-Fe

DPPH assay: Cur-Fe was prepared at different concentrations and mixed with 125 μM DPPH in the same volume of ethanol. The final concentrations of Cur-Fe were 1, 2.5, 5, 10, and 20 $\mu\text{g}/\text{mL}$. The absorbance of DPPH was measured at 517 nm 30 min after the end of the reaction.

ABTS assay: Equal volumes of ABTS solution and oxidant solution were mixed well to form the ABTS masterbatch, which was stored at room temperature and protected from light for 16 h. Then, the ABTS masterbatch was diluted 50-fold with PBS solution to form the ABTS working solution, and 10 μL of different concentrations (20 $\mu\text{g}/\text{mL}$, 50 $\mu\text{g}/\text{mL}$, 100 $\mu\text{g}/\text{mL}$, 200 $\mu\text{g}/\text{mL}$, and 400 $\mu\text{g}/\text{mL}$) of the Cur-Fe solution and the 190 μL of the ABTS working solution were mixed and then incubated at room temperature for 5 min to measure the absorbance at 734 nm.

TMB assay: 10 μM FeCl_2 solution, 50 μM H_2O_2 solution, and 300 μM TMB solution were prepared with ultrapure water. Then, 100 μL of each of the above three solutions were homogeneously mixed, and then 10 μL of Cur-Fe solution with different concentrations (30 $\mu\text{g}/\text{mL}$, 75 $\mu\text{g}/\text{mL}$, 150 $\mu\text{g}/\text{mL}$, 300 $\mu\text{g}/\text{mL}$, and 600 $\mu\text{g}/\text{mL}$) and the 290 μL mixed system were well mixed, and then the absorbance was measured at 645 nm after 30 min of reaction at room temperature.

BMPO assay: Electron spin resonance (ESR) is a resonance absorption signal generated by the absorption of microwave energy by an electron spin in a magnetic field. BMPO works as the trapper of $\text{O}_2^{\cdot-}$ radicals generated by the reaction of hypoxanthine (HYP) with xanthine oxidase (XOD). The reaction system was placed at 37 $^\circ\text{C}$ for 15 min and the signal changes were recorded using ESR (EPR 200 M, CIQTEK Co., Ltd.).

Cell culture

RAW 264.7 and FHC cells were cultured in DMEM medium supplemented with 10% fetal bovine serum (FBS), 100 U/mL penicillin, and streptomycin at 37 $^\circ\text{C}$ and 5% CO_2 .

Intracellular ROS scavenging

After 2.5 $\mu\text{g}/\text{mL}$ Cur or Cur-Fe were cocultured with RAW 264.7 cells for 8 h, different concentrations of H_2O_2 were added to the medium to continue the cocultivation for 4 h, the medium was removed, and 0.5 mg/mL MTT solution was added to continue the incubation for 4 h. The MTT solution was then aspirated, and 150 μL DMSO solution was added to the cells with shaking for 10 min, and the absorbance was measured at 490 nm.

After 2.5 $\mu\text{g}/\text{mL}$ of Cur or Cur-Fe were co-cultured with RAW 264.7 cells for 8 h, 200 μM of H_2O_2 was added to the medium to continue co-cultivation for 1 h, then the medium was removed and incubated with 10 μM of DCFH-DA solution or 1 μM of DHE solution for 1 h. The medium was aspirated and washed three times with PBS, and then observed by fluorescence microscopy or quantified by flow cytometry.

First, RAW 264.7 cells were co-cultured with 2.5 $\mu\text{g}/\text{mL}$ of Cur or Cur-Fe for 8 h. Then 500 μM of H_2O_2 was added to continue the incubation for 4 h. At the end of the time, the medium was aspirated and supplemented with calcein-AM/PI for 1 h. The medium was washed with PBS and finally placed in the fluorescence microscope for observation. Alternatively, the medium was aspirated and discarded after 4 h. The incubation was continued by adding Annexin V-FITC/PI for 15 min at 25 $^\circ\text{C}$, protected from light, and finally quantified by flow cytometry.

Intracellular anti-inflammatory effect

After 2.5 $\mu\text{g}/\text{mL}$ of Cur or Cur-Fe were co-cultured with RAW 264.7 cells for 8 h, 500 ng/mL of LPS was added to the medium to continue co-cultivation for 8 h. The cells were then harvested, RNA was extracted, and the expression of inflammatory factor mRNA was detected by qPCR after reverse transcription. Alternatively, cells were harvested after LPS induction, washed three times with PBS, incubated with 200 μL of CD86 for 30 min at 4 $^\circ\text{C}$, washed three times with PBS, and detected by flow cytometry.

Preparation of DiL-labeled Cur-Fe and CF@EM for cellular uptake experiments. DiL-labeled Cur-Fe was prepared by stirring 20 μL of 10 mM DiL with 1 mg/mL Cur-Fe overnight, followed by centrifugation at 5000 g for 10 min, and then resuspending the precipitate. DiL-labeled CF@EM was prepared by combining DiL-labeled Cur-Fe with EM according to the same method as that used to prepare CF@EM earlier. The same concentrations of DiL-labeled Cur-Fe and DiL-labeled CF@EM

were incubated with RAW264.7 cells at different times respectively. Subsequently, the cells were washed three times with PBS and detected by flow cytometry.

Intestinal colonization of CF@EM

DiR-labeled Cur-Fe and CF@EM were prepared for intestinal colonization experiments. The DiR-labeled Cur-Fe and CF@EM were prepared using the same methodology as that employed for the DiL-labeled Cur-Fe and DiL-labeled CF@EM, as previously described. Then mice were given the same concentration of DiR-labeled Cur-Fe and DiR-labeled CF@EM orally. Meanwhile, the fluorescence intensity of mice was calculated at different time points. The mice were sacrificed after 12 h and the fluorescence intensity of each tissue was counted. The mice were also given 3% DSS to establish the UC model, and the differences in the distribution of different oral agents in the body and tissues of mice were observed according to the same protocol.

Animals

C57/BL6 female mice (8 weeks old) were provided by the Medical Experimental Animal Center of Xi'an Jiaotong University, Shaanxi Province, China. All animal procedures were performed following the Guidelines for Care and Use of Laboratory Animals of Xi'an Jiaotong University and approved by the Animal Ethics Committee.

Biocompatibility and biosafety evaluation

RAW 264.7 cells and FHC cells were co-cultured with different concentrations of Cur-Fe for 24–48 h. The biosafety of Cur-Fe at the cellular level was evaluated by MTT assay.

To test the biocompatibility of Cur-Fe and CF@EM *in vivo*, mice were orally administered 30 mg/kg of Cur-Fe and CF@EM per day. On day 8, mice were necropsied and blood was collected for routine hematology and biochemical analysis. Hearts, livers, spleens, lungs, and kidneys were collected and fixed in 4% paraformaldehyde (PFA) and stained with hematoxylin-eosin (H&E) to observe histologic changes.

DSS-induced colitis of mice

C57BL/6 mice (6–8 weeks) were used to build the colitis mice model. Mice were randomly grouped into groups of at least 6 mice each. After 1 week of acclimatization, 2.5% DSS was given for 7 consecutive days to induce acute colitis in mice, and different preparations (30 mg/kg of Cur, Cur-Fe, and CF@EM; 40 mg/kg of 5-ASA) were administered orally for 5 consecutive days after 7 days. Bodyweight, stool characteristics, and blood in the stool were recorded daily and a total score was taken to determine DAI. Each parameter was scored as follows: body weight loss (0=<1%, 1=1–5%, 2=5–10%, 3=10–20%,

4=>20%), the presence or absence of blood in the feces (0=negative, 2=hidden blood in stool, 4=bloody stool), and stool consistency (0=normal stool, 1=soft stools, 2=loose stools, 3=diarrhea). The mice were executed on the last day of the experiment, and the distal colon was taken for subsequent experimental analysis.

To verify the preventive effect of CF@EM on colitis, 2.5% DSS was administered for 7 consecutive days to induce acute colitis in mice. Different preparations were administered orally on days 1, 3, 5, and 7, and other treatments were as above. All the experiments were conducted following the Institutional Animal Care and Use Committee of Xi'an Jiaotong University.

Immunofluorescence analysis

Colon tissue was embedded in optimal cutting temperature compound made into frozen section and washed 3 times with PBS for 5 min each. 4% PFA was fixed for 10 min and also washed 3 times with PBS. Then CD86 antibody was added and incubated at 4 °C overnight. Alternatively, a DHE fluorescent probe was added and incubated at room temperature for 30 min. At the end of the time, the sections were washed 3 times with PBS, sealed with DAPI, and observed by fluorescence microscopy.

Sections were fixed with pre-cooled ethanol at -20 °C or 4% PFA for 10 min at room temperature. Sections were rinsed with PBS 3 times for 5 min each. They were incubated with 0.2% Triton X-100 for 5 min at room temperature. Rinse 3 times with PBS for 5 min each. Incubate with blocking buffer for 1 h at room temperature. Remove the blocking buffer and incubate with tight junction protein primary antibody overnight at 4 °C. Wash 3 times with PBS for 5 min each and visualize by fluorescence microscopy after DAPI sealing.

Statistical analysis

All results were statistically analyzed using GraphPad Prism 9.0 software. Student's *t*-test was used to compare the two groups. Results are expressed as mean ± standard deviation (SD), *p*<0.05 indicates a statistically significant difference.

Results and discussion

Synthesis and characterization of Cur-Fe and CF@EM

Cur-Fe was synthesized by dropwise addition of curcumin (Cur) to a mixture of FeCl₃ and polyvinylpyrrolidone (PVP). The obtained Cur-Fe significantly improved the solubility and dispersion of curcumin in water (Fig. S1A). The morphology of Cur-Fe was characterized using transmission electron microscopy (TEM), revealing a uniform morphology and a size of approximately 5 nm. Energy dispersive spectrometer (EDS) results showed irregular doping of a significant amount of C,

O, and Fe in Cur-Fe, suggesting that these elements are the main components of Cur-Fe (Fig. 2A). X-ray diffraction (XRD) analysis further confirmed that Cur-Fe is amorphous (Fig. S1B). Fluorescence emission spectra were obtained for both curcumin and Cur-Fe at an excitation wavelength of 400 nm. The results demonstrated that curcumin exhibited remarkable fluorescence at 520 nm, whereas Cur-Fe showed significant quenching (Fig. 2B). This quenching effect can be attributed to the complexation between curcumin and the metal ion, leading to non-radiative charge transfer. Fourier transform infrared (FTIR) spectra of Cur-Fe also indicated the coordination of ferric ions with the HO-C group in curcumin, as evidenced by the reduced infrared intensity at 1150–1200 cm^{-1} (HO-C stretching band) (Fig. 2C). UV-Vis results revealed that Cur-Fe exhibited a maximum absorption wavelength similar to that of Cur, as

well as a characteristic absorption peak similar to that of FeCl_3 (Fig. S1C). These findings collectively suggest the formation of a stable complex between Cur and iron ions in the nanomaterials. X-ray photoelectron spectroscopy (XPS) analysis was performed to determine the elemental valence state of ferric ions in the nanomaterials, which showed the coexistence of Fe^{2+} and Fe^{3+} states (Fig. 2D). To obtain CF@EM, EM was added to Cur-Fe under ultrasound. TEM results showed that a large number of black particles were visible in CF@EM (Fig. 2A), indicating that Cur-Fe was successfully encapsulated in EM. Similarly, SDS-PAGE results showed that the protein profile in CF@EM was consistent with that in EM (Fig. 2E). Dynamic light scattering (DLS) results showed that the size of Cur-Fe nanoparticles encapsulated with EM increased from 19.12 ± 1.66 nm to 200.16 ± 17.35 nm (Fig. 2F), and the zeta potential decreased from

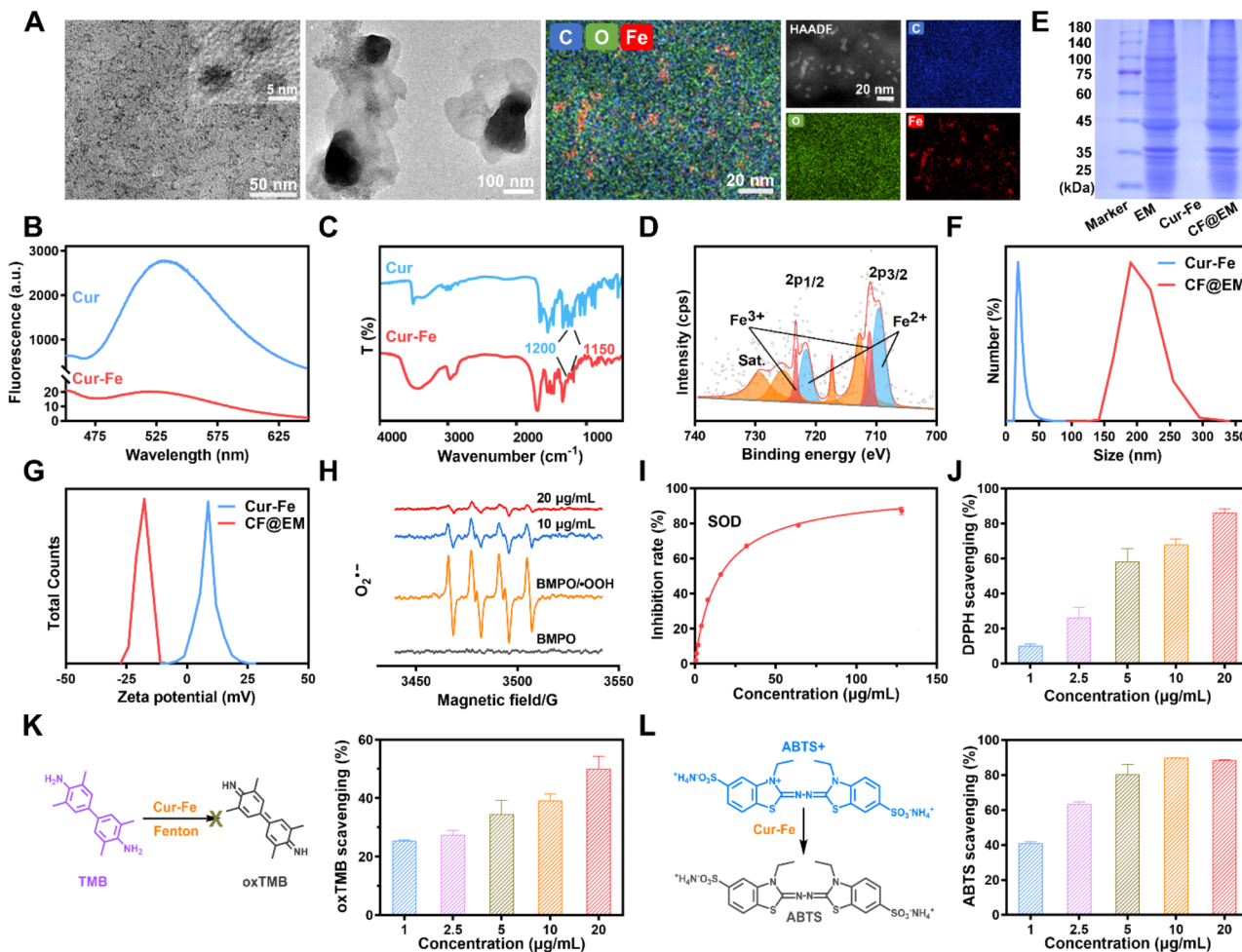


Fig. 2 Characterization and ROS scavenging activities. **(A)** TEM images of Cur-Fe and CF@EM. The image on the right shows the element mapping of Cur-Fe. **(B)** The fluorescence of curcumin and Cur-Fe. **(C)** FTIR of curcumin and Cur-Fe. **(D)** XPS of Cur-Fe. **(E)** SDS-PAGE protein analysis of EM, Cur-Fe, and CF@EM. **(F)** Particle size distribution of Cur-Fe and CF@EM. **(G)** Zeta-potential of Cur-Fe and CF@EM. **(H)** ESR spectra of BMPO indicating $\text{O}_2^{\cdot-}$ scavenge with Cur-Fe. **(I)** SOD assay kit to determine the SOD-like activity of Cur-Fe. **(J)** DPPH radical scavenging ratio of Cur-Fe. **(K)** Schematic illustration of the TMB + $\cdot\text{OH}$ scavenging process and the scavenging ratio of Cur-Fe. **(L)** Schematic illustration of the ABTS radical scavenging process and the scavenging ratio of Cur-Fe. Data were expressed as the mean \pm SD ($n=3$)

9.28±0.88 mV to -13.81±0.59 mV (Fig. 2G, S1D). All these results indicated that CF@EM was successfully synthesized. Concurrently, the size of Cur-Fe and CF@EM were measured over seven days, and no significant changes were observed. This suggests that both Cur-Fe and CF@EM exhibit good stability (Fig. S1E).

Enzymatic activities of Cur-Fe

Since polyphenols are usually considered natural antioxidants, to verify the antioxidant capacity of Cur-Fe, we evaluated its enzymatic activity. $O_2^{\cdot-}$ is one of the common free radicals, and hypoxanthine/xanthine oxidase (HYP/XOD) can produce $O_2^{\cdot-}$, because $O_2^{\cdot-}$ is extremely unstable and exists for a very short period, BMPO was employed as a trapping agent to capture the produced $O_2^{\cdot-}$ and form a more stable (BMPO/ \bullet OOH) spin adduct. Electron spin resonance (ESR) spectroscopy revealed that the $O_2^{\cdot-}$ produced by HYP/XOD could be effectively scavenged by Cur-Fe (Fig. 2H). Nitro-blue tetrazolium (NBT) is a commonly used $O_2^{\cdot-}$ tracer that reacts with $O_2^{\cdot-}$ to form water-insoluble formazan, and the $O_2^{\cdot-}$ scavenging ability can be measured by determining the absorbance of formazan at 560 nm. It was found that Cur-Fe had nearly 90% $O_2^{\cdot-}$ removal at a concentration of 20 μ g/mL (Fig. S2). The SOD enzyme activity of Cur-Fe was evaluated by testing with a commercially available SOD assay kit. It was found that Cur-Fe has a good $O_2^{\cdot-}$ scavenging ability with an enzyme activity of 269 U/mg (Fig. 2I). The 1,1-diphenyl-2-picrylhydrazyl (DPPH) radical, one of the widely used models in free radical scavenging assays, is a very stable nitrogen-centered radical. The results showed that a lower concentration of Cur-Fe exhibited excellent DPPH radical scavenging ability (Fig. 2J). 3,3',5,5'-Tetramethylbenzidine (TMB) is a commonly used \bullet OH chromogenic substrate, and the \bullet OH generated by the Fenton reaction can oxidize the TMB to oxTMB, and the Cur-Fe can reduce the oxTMB (Fig. 2K). Similarly, 2,2'-Azinobis-(3-ethylbenzthiazoline-6-sulfonate) (ABTS) was commonly used as a chromogenic substrate to detect the scavenging effect of ROS as a function of the total antioxidant capacity of the nanoparticles. The results showed that Cur-Fe with a lower concentration (5 μ g/mL) could scavenge ~80% ROS, thus exhibiting excellent antioxidant capacity (Fig. 2L).

The intracellular anti-inflammatory and antioxidant effects of Cur-Fe

Under oxidative stress, such as stimulation with high concentrations of H_2O_2 , cells generate large amounts of ROS. 2,7-dichlorofluorescein diacetate (DCFH-DA) is a cell-permeable probe. It will be hydrolyzed to DCFH when it enters the cells, and non-fluorescent DCFH will be oxidized to fluorescent DCF by intracellular ROS. With H_2O_2 stimulation, strong green fluorescence

appeared in the cells, indicating a large amount of ROS generated under the oxidative stress state. In contrast, the green fluorescence was attenuated by pretreatment with Cur and Cur-Fe (Fig. 3A). Flow cytometry results further showed that Cur and Cur-Fe significantly reduced ROS levels, and the scavenging ability of Cur-Fe was superior (Fig. 3B, S3A). To verify the $O_2^{\cdot-}$ scavenging ability of Cur-Fe, dihydroethidium (DHE) was used to detect intracellular $O_2^{\cdot-}$ levels after H_2O_2 treatment. Similar to DCF, a large amount of red fluorescence was produced in the cells after H_2O_2 stimulation, which was attenuated by pretreatment with Cur and Cur-Fe, and the scavenging capacity of Cur-Fe was superior to that of Cur (Fig. 3C). The flow cytometry results were consistent with the fluorescence images (Fig. 3D, S3B).

Excessive oxidative stress can induce oxidative damage and cell death. To verify the protective ability of Cur-Fe against H_2O_2 -induced cellular oxidative damage, calcein-AM/PI was used to detect the cellular status. Calcein-AM can easily penetrate the cell membrane of living cells and emit strong green fluorescence, while PI can only penetrate dead cells and emit red fluorescence. After induction by H_2O_2 , a proportion of cells died due to oxidative stress, and the number of dead cells decreased after treatment with Cur and Cur-Fe (Fig. 3E). Detection of cell viability by methylthiazolyl tetrazolium (MTT) further indicated that Cur and Cur-Fe significantly increased cell viability after induction with different concentrations of H_2O_2 , and the protective effect of Cur-Fe on cells was more pronounced (Fig. S4). Quantification of Annexin V-FITC/PI by flow cytometry showed that Cur-Fe inhibited H_2O_2 -induced apoptosis and thus enhanced cell viability (Fig. 3F, G).

Inflammation is often accompanied by oxidative stress in the processes associated with inflammatory diseases. Lipopolysaccharides (LPS) can induce a variety of cytokines and inflammatory mediators in vivo by activating macrophages, endothelial cells, and epithelial cells through cell signaling systems. Therefore, we used LPS to induce RAW 264.7 cells in vitro to simulate the acute inflammatory state. The relative expression of TNF- α , IL-6, IL-12, and IL-1 β was determined by real-time quantitative polymerase chain reaction (qPCR). The expression of cellular inflammatory factors was found to be increased after LPS induction, whereas it was significantly decreased in both Cur and Cur-Fe groups compared with the LPS group, with expected, a more pronounced decrease in the Cur-Fe group (Fig. 3H). Similarly, the ability of Cur-Fe to scavenge LPS-induced ROS was verified by incubating a DCFH-DA fluorescent probe to detect ROS generation in cells after LPS stimulation. The results showed that the LPS group induced a higher ROS generation, while both Cur and Cur-Fe groups reduced ROS generation (Fig. S5A). Flow cytometry

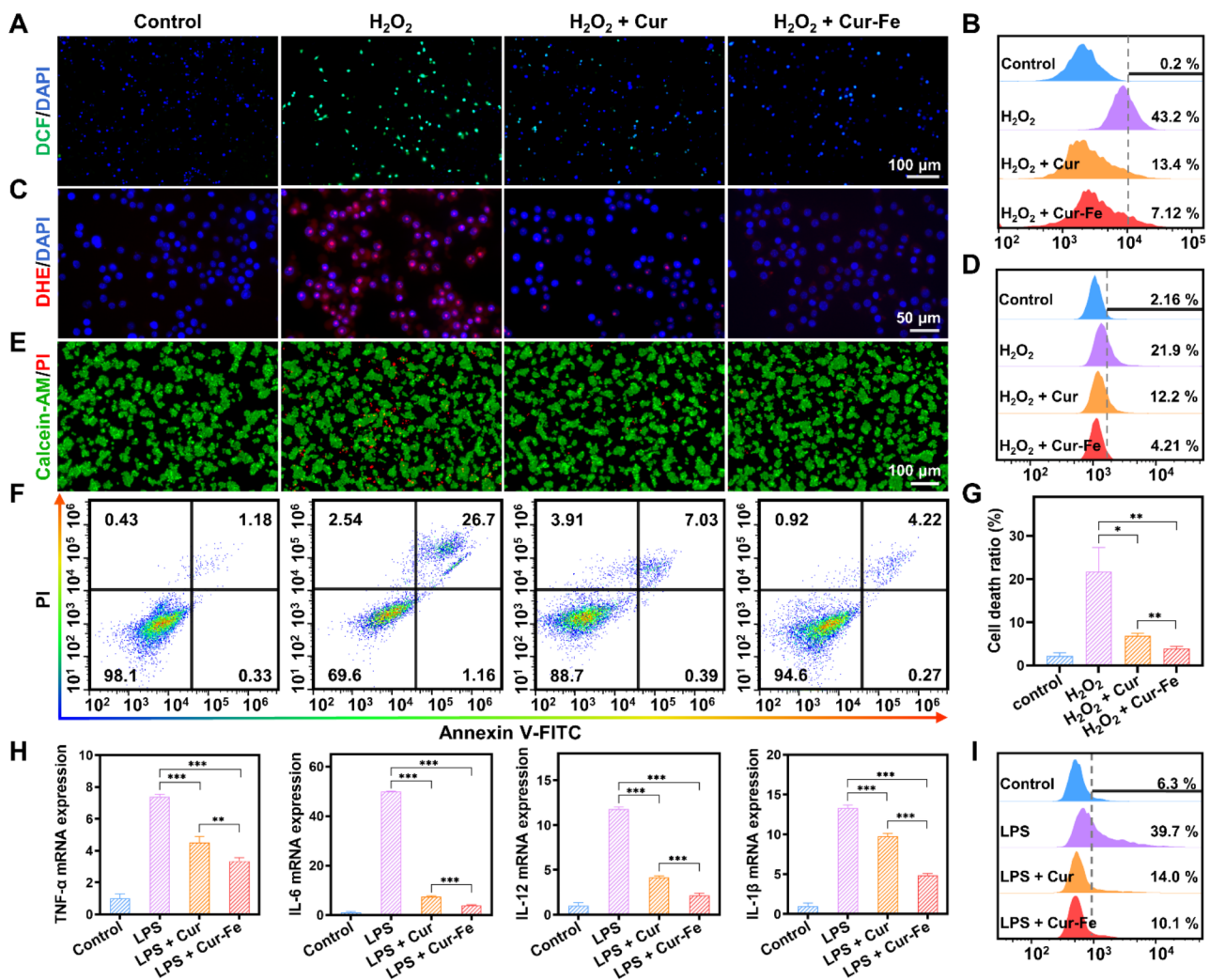


Fig. 3 Anti-inflammatory and antioxidant effects of Cur-Fe in vitro. **(A, B)** Fluorescence images **(A)** and flow cytometry quantification **(B)** of DCF stained RAW 264.7 cells after different treatments. **(C, D)** Fluorescence images **(C)** and flow cytometry quantification **(D)** of DHE. **(E)** Fluorescence images of calcein-AM/PI. **(F)** Flow cytometry quantification of Annexin V-FITC/PI. **(G)** The cell death ratio was calculated based on the flow cytometry data in **(F)**. **(H)** The mRNA expression of inflammatory cytokines (TNF- α , IL-6, IL-12, and IL-1 β) in different groups. **(I)** Quantitative assessment of M1 macrophages after different treatments by flow cytometry. Data were expressed as the mean \pm SD ($n=3$). Statistical analysis was performed using a two-tailed Student's *t*-test. * $P < 0.05$, ** $P < 0.01$, and *** $P < 0.001$, represented different statistical significances, and ns represents no statistical difference

results showed that Cur and Cur-Fe had similar scavenging abilities for LPS-induced ROS generation (Fig. S5B, C). The complex tissue microenvironment can lead to macrophage activation and polarization into functionally distinct subpopulations, and LPS induction usually converts macrophages into M1 macrophages, which promotes inflammation [32]. The effect of Cur-Fe on macrophage polarization was verified by observing changes in cell morphology and detecting CD86 overexpression on the surface of M1 macrophages. The results of cell morphology showed that Cur and Cur-Fe inhibited macrophage morphology alteration (Fig. S6A). The results of flow cytometry similarly showed that Cur and Cur-Fe inhibited the conversion of macrophages into pro-inflammatory M1 macrophages (Fig. 3I, S6B), thereby reducing

the expression of inflammatory mediators and alleviating cellular inflammation. Meanwhile, we compared the uptake of Cur-Fe and CF@EM at the cellular level. The cellular uptake of Cur-Fe and CF@EM was also compared, and the results demonstrated that the delivery of Cur-Fe by EM enhanced the cellular uptake of Cur-Fe, as indicated by the increased fluorescence intensity of CF@EM observed in the first hour. Furthermore, the fluorescence intensities of Cur-Fe and CF@EM were found to be similar at the three-hour mark, suggesting that the cellular uptake of Cur-Fe had already saturated by then (Fig. S7). The presence of EM was observed to have no impact on the efficiency of Cur-Fe uptake by cells but rather reduced the time required for saturation to be reached.

Intestinal colonization of CF@EM

Due to the complex environment of the gastrointestinal tract, oral drug delivery will encounter the degradation and absorption of drugs in the stomach and small intestine, resulting in low drug concentrations in the colon, and shortened drug residence time due to the peristaltic function of the intestinal tract, which should be the potential causes of suboptimal drug therapy. To verify intestinal colonization after Cur-Fe-coated EM, Cur-Fe and CF@EM were administered to normal mice and DSS-induced colitis mice, respectively, and then their *in vivo* distribution was dynamically observed. In normal mice, Cur-Fe was completely cleared from the body within 12 h, whereas CF@EM still had a strong fluorescence signal after 12 h, indicating that CF@EM was more retained in normal mice (Fig. 4A, B). Similar results were observed in the UC model. Although the altered gastrointestinal motility of the diseased mice resulted in less Cur-Fe being incompletely cleared from the body at 12 h, CF@EM still showed a strong *in vivo* retention capacity

(Fig. 4A, C). When the isolated tissues were examined, it was found that CF@EM remained almost entirely in the intestine, with the cecum and colon regions predominating, while CF@EM distribution was not detected in other tissues and organs (Fig. 4A). Compared with the Cur-Fe group, the retention time significantly improved in the CF@EM group, and similar results were found in both the normal model and the inflammatory condition, suggesting that CF@EM has a better colonization effect on intestinal tissues (Fig. 4D).

Biosafety assessment of Cur-Fe and CF@EM

For the *in vivo* use of Cur-Fe and CF@EM, appropriate biosafety evaluations should be performed. The effects of Cur-Fe and CF@EM on the viability of RAW 264.7 and FHC cells were determined by MTT. The results showed that cell viability was still around 80% after incubation of 200 $\mu\text{g}/\text{mL}$ Cur-Fe or CF@EM with RAW 264.7 cells for 24 and 48 h. Similarly, the same concentration of Cur-Fe

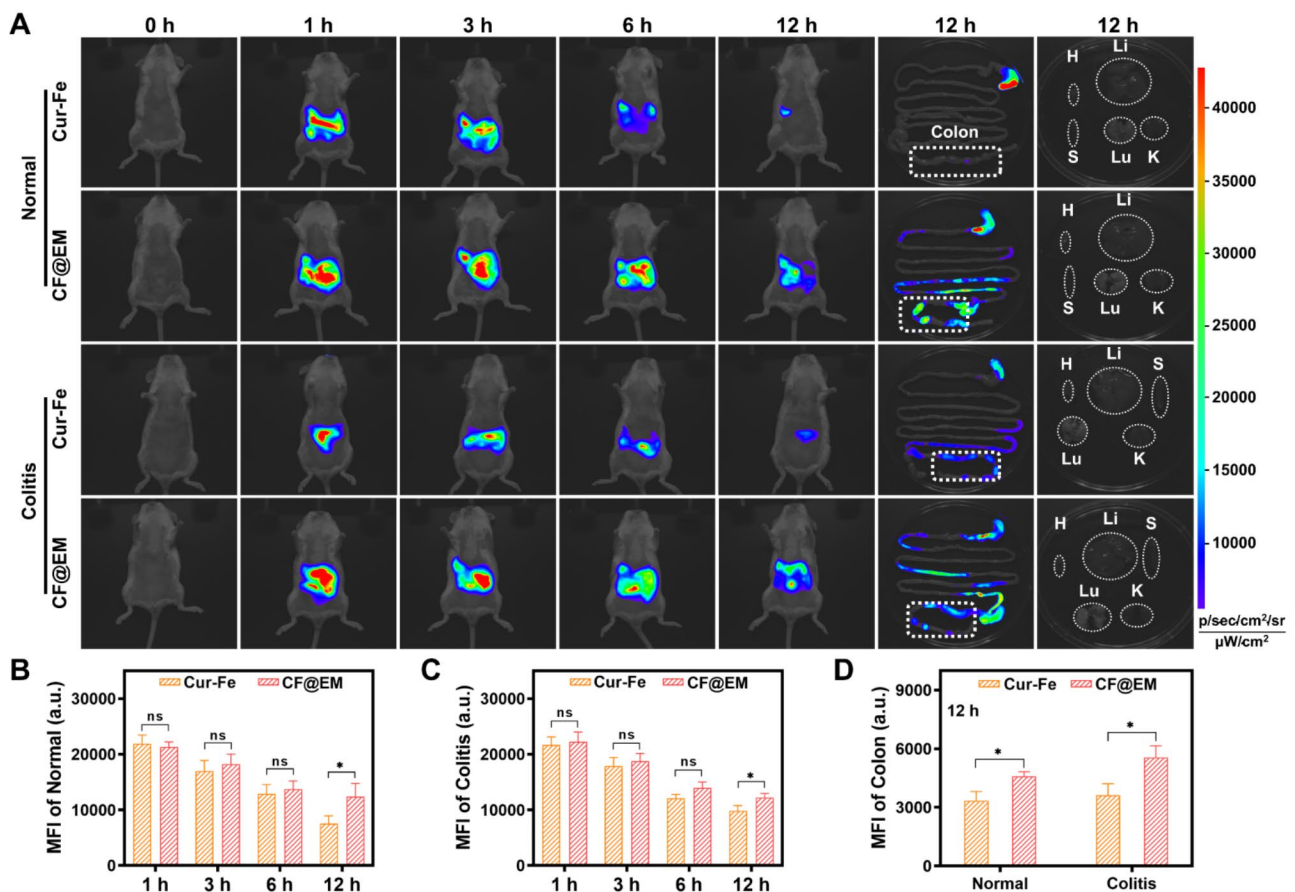


Fig. 4 Intestinal colonization of CF@EM. **(A)** Fluorescence images of normal mice, DSS-induced colitis mice, colon tissues, and organs at indicated time points after oral Cur-Fe and CF@EM. H: heart; Li: liver; S: spleen; Lu: lung; K: kidney. **(B, C)** Quantification of mean fluorescence intensity in normal **(B)** and DSS-induced colitis mice **(C)** *in vivo*. **(D)** Quantification of mean fluorescence intensity in colon tissues of normal and DSS-induced mice. Data were expressed as the mean \pm SD ($n=3$). Statistical analysis was performed using a two-tailed Student's *t*-test. * $P<0.05$, ** $P<0.01$, and *** $P<0.001$, represented different statistical significances, and ns represents no statistical difference

or CF@EM was incubated with FHC cells for the same time, and cell viability remained above 80% (Fig. S8A).

After oral administration of Cur-Fe and CF@EM, no significant pathological changes in mice were found in H&E staining major tissue sections (Fig. S8B). Meanwhile, red blood cells, white blood cells, lymphocytes, platelets, and hemoglobin were examined, and the results showed that there were no significant differences between mice in the Cur-Fe and CF@EM groups and mice in the control group (Fig. S8C). Similarly, to evaluate the changes in biochemical indices, alanine aminotransferase (ALT) and aspartate aminotransferase (AST) were used as liver function evaluation indices, and creatinine (CRE) and urea were used as renal function indices, and it was found that both Cur-Fe group and CF@EM group showed no significant differences compared with the control group (Fig. S8C). It was demonstrated that both Cur-Fe and CF@EM had good biosafety.

Therapeutic efficacy of CF@EM in DSS-induced colitis

Based on the intestinal colonization effect of CF@EM and the anti-inflammatory and antioxidant effects of

Cur-Fe, we evaluated the therapeutic effect of CF@EM in a DSS-induced ulcerative colitis model. Based on the results of the biosafety assessment, we decided to administer Cur-Fe and CF@EM at a dose of 30 mg·kg⁻¹. To better evaluate the therapeutic effect of CF@EM, we selected 5-aminosalicylic acid (5-ASA), a clinically used therapeutic drug, as a positive drug control group. At the end of 7 days of modeling, drug treatment was administered for 5 consecutive days (Fig. 5A). The results showed that the mice in the control group showed a trend of slow increase in body weight and no significant change in disease activity index (DAI), while the DSS group showed a gradual decrease in body weight with the progression of the disease, and the DAI was maintained at a high level after continuously increasing, indicating that the disease progression was more serious. Compared with the DSS group, the remaining four groups showed a moderation in the degree of weight loss and increase in DAI, especially the 5-ASA group and the CF@EM group showed a rebound in body weight and a significant decrease in DAI after treatment, indicating that the disease was effectively controlled (Fig. 5B, C). Endoscopic examination

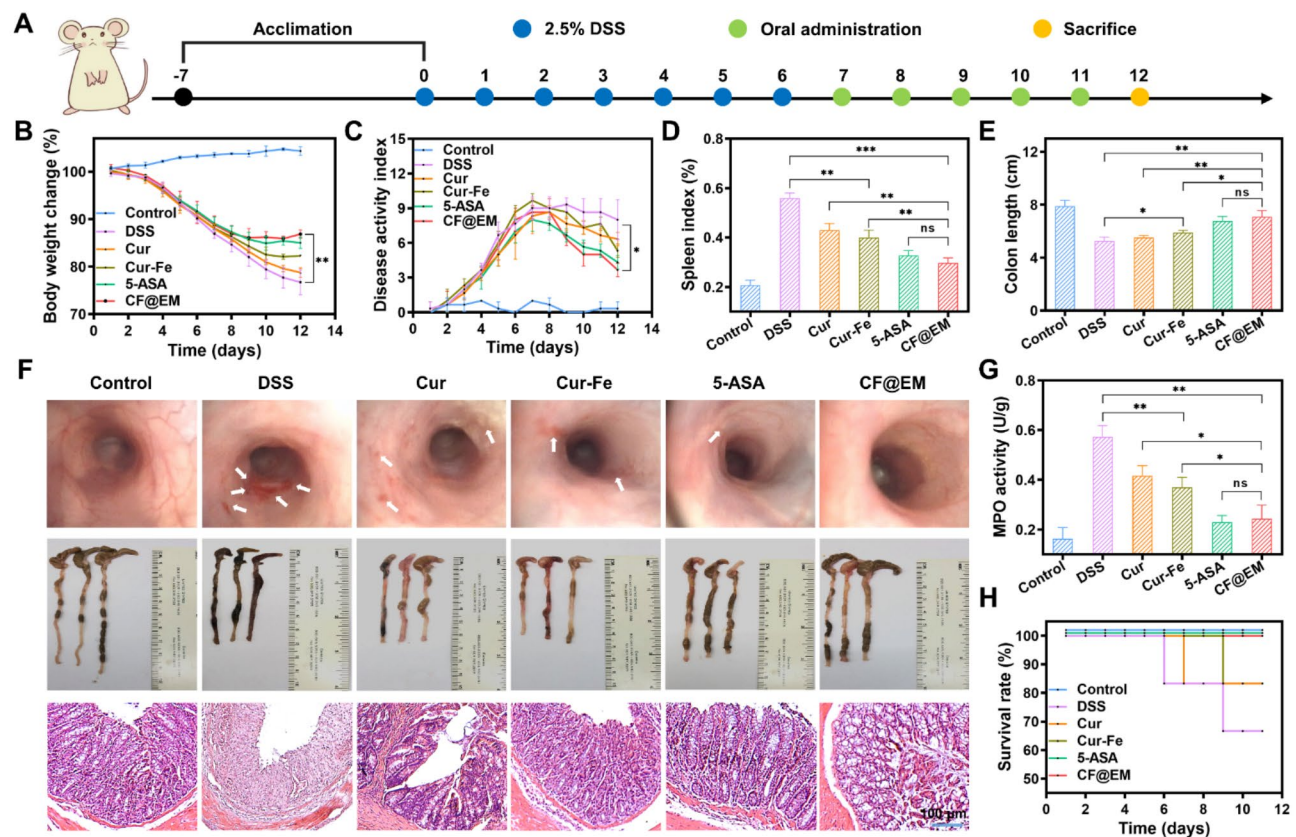


Fig. 5 Therapeutic efficacy of CF@EM in DSS-induced colitis. **(A)** Schematic illustration of the establishment and treatment of DSS-induced colitis mice. **(B, C)** Weight change curves **(B)** and DAI curves **(C)** of mice within 12 days. **(D)** The spleen index of mice in different treatment groups. **(E)** The length of the colon. **(F)** Endoscopic images, colon images, and H&E staining of mice in different treatment groups. **(G)** The MPO activity of mice. **(H)** The survival rate of mice in different treatment groups. Data were expressed as the mean \pm SD ($n = 3$). Statistical analysis was performed using a two-tailed Student's *t*-test. * $P < 0.05$, ** $P < 0.01$, and *** $P < 0.001$, represented different statistical significances, and ns represents no statistical difference

of the mice revealed that the intestinal mucosa of mice in the DSS group showed diffuse ulceration with hemorrhage, and the intestines were significantly improved after treatment with CF@EM, and the effect was superior to that of Cur-Fe. The evaluation of spleen index and colon length showed that the CF@EM group could significantly reduce the spleen index and restore the colon length, which was not significantly different from that of the 5-ASA group, while the simple Cur-Fe group had some therapeutic effect, but the efficacy was limited (Fig. 5D-F). In the H&E staining of the colon, it could be seen that all the epithelial cells and crypts were destroyed in the DSS group, and also showed obvious inflammatory cell infiltration; the Cur and Cur-Fe groups preserved part of the crypts and epithelial cell structure, and the lesion area was reduced. The CF@EM group significantly reduced the pathological damage of the colon (Fig. 5F). By myeloperoxidase (MPO) detection, it was found that both Cur-Fe and CF@EM could reduce the MPO level, and the effect of CF@EM was more significant (Fig. 5G). As the disease progresses, mice with more severe symptoms may die. Therefore, the survival rate of each group was counted. It was found that except for the 5-ASA group and the CF@EM group, the survival rates of the other groups modeled by DSS were reduced (Fig. 5H).

CF@EM relieves inflammation and restores intestinal barrier function

The production of inflammatory cytokines is very important in the development of colitis. The detection of pro-inflammatory cytokines revealed that TNF- α , IL-6, IL-1 β , and IL-12 were highly expressed in the DSS group, whereas Cur-Fe and CF@EM reduced the expression of pro-inflammatory cytokines, and the anti-inflammatory effect of the CF@EM group was significantly superior to that of Cur-Fe. The CF@EM group showed the same anti-inflammatory capacity compared with the 5-ASA group (Fig. 6A-D). Inflammatory cell infiltration is usually one of the tissue features of colitis, and by immunofluorescence staining for CD86, a surface marker of M1 macrophages, we observed a large amount of red fluorescence in the colon of the DSS group. The expression of CD86 in the colon was dramatically downregulated after Cur-Fe and CF@EM interventions (Fig. 6E). These results suggest that Cur-Fe and CF@EM can modulate macrophage polarization and reduce M1 macrophages that promote inflammatory responses, which helps to slow down the development of colitis.

ROS typically accumulate in large amounts at sites of inflammation and cause oxidative damage to cells. Fluorescence staining with DHE was performed to evaluate $O_2^{\bullet-}$ generation in colon tissues. The results showed that obvious red fluorescence was observed in the DSS group, indicating that DSS induced the generation of a large

amount of $O_2^{\bullet-}$, whereas the fluorescence intensity was attenuated in the Cur-Fe group and the CF@EM group, and $O_2^{\bullet-}$ was effectively removed (Fig. 6F). These results suggest that CF@EM can alleviate tissue damage during the development of colitis by reducing intestinal ROS levels.

The intestinal barrier is an important barrier that prevents harmful substances and pathogens from entering the body and maintains intestinal homeostasis [33, 34]. The paracellular permeability of the intestinal barrier depends on tight junctions (TJ) between cells. By immunofluorescence staining of three tight junction proteins, occludin, ZO-1, and claudin-1, we observed the changes in tight junctions after different treatments. It was found that the fluorescence of all three tight junction proteins was weak in the DSS group and increased slightly after Cur-Fe intervention. In contrast, the fluorescence intensity was restored to almost normal levels in the CF@EM group (Fig. 6G), indicating that CF@EM can improve intestinal barrier function by restoring intercellular tight junctions.

Preventive effect of CF@EM in DSS-induced colitis

To further validate the preventive effect of CF@EM, four groups of mice were intermittently administered different preparations of the intervention over 7 days of oral DSS modeling (Fig. 7A). The results were as expected, with rapid weight loss and higher DAI scores in the DSS group, indicating faster disease progression and more severe symptoms. In contrast, the CF@EM group had almost no significant change in body weight and lower DAI scores, which were significantly different from the DSS group (Fig. 7B, C). Observation of feces and endoscopy revealed that the DSS group had dilute liquid-like feces with obvious bleeding. The intestinal mucosa had multiple ulcers and was significantly shorter in length. Fecal status and ulceration were significantly improved after intervention with various agents, along with some restoration of spleen index and colon length. In particular, the severity of colitis in mice was almost maintained at a milder level in the presence of CF@EM. There were significant differences compared with both Cur-Fe and 5-ASA groups (Fig. 7D-F). H&E staining revealed that the colonic crypts and epithelial cell structure were less damaged in the CF@EM group, further confirming that CF@EM had a beneficial effect on inhibiting the development of colitis (Fig. 7F). After the detection of three pro-inflammatory cytokines, it was found that the expression of TNF- α , IL-6, and IL-1 β was significantly downregulated in both Cur-Fe and CF@EM groups. It indicated that CF@EM had an inhibitory effect on the development of inflammation and was significantly better than Cur-Fe and 5-ASA (Fig. 7G).

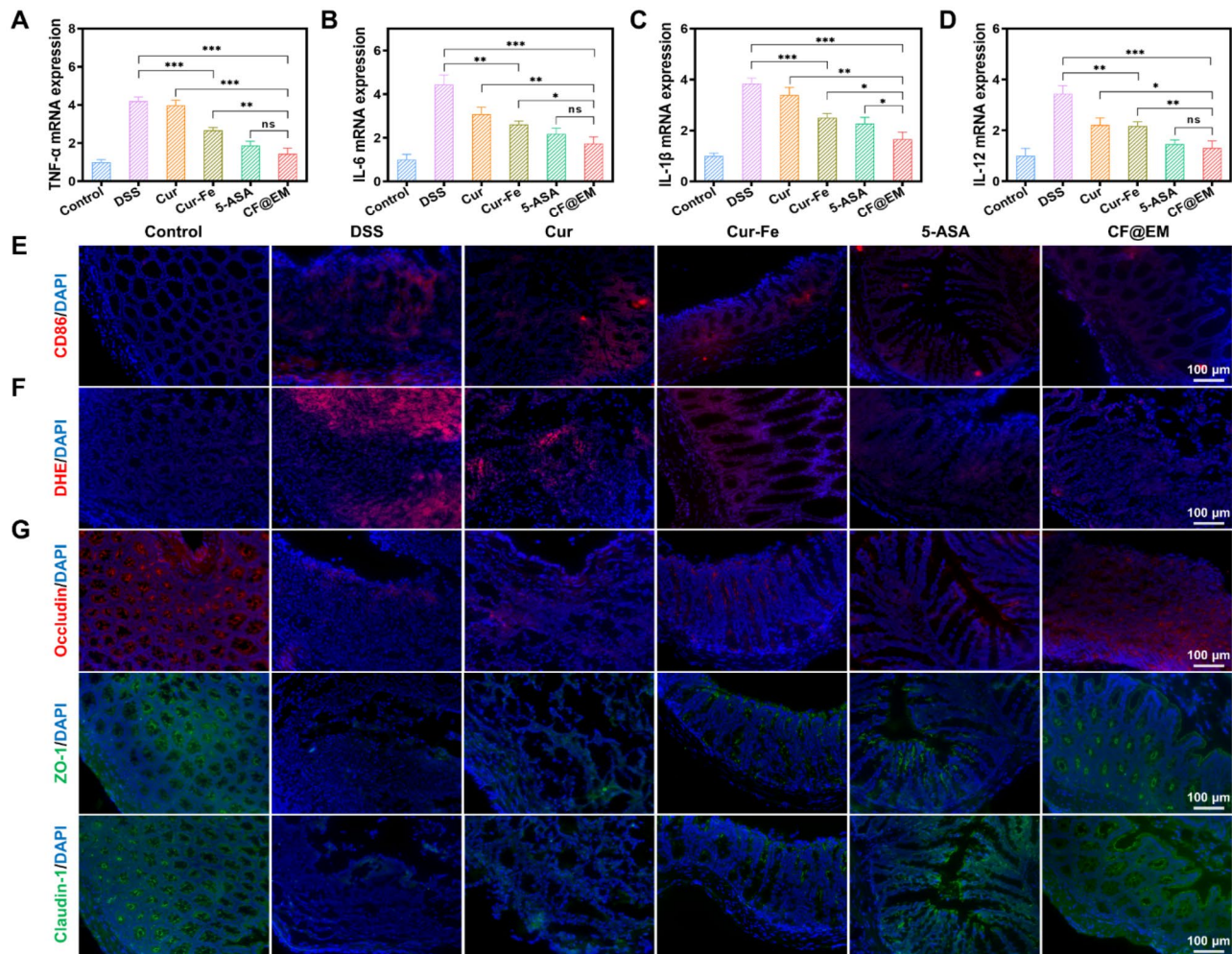


Fig. 6 CF@EM relieves inflammation and restores intestinal barrier function. (A–D) The mRNA expression of TNF- α (A), IL-6 (B), IL-1 β (C), and IL-12 (D) in different groups. (E) Evaluation of the M1 macrophage in the colon of the colitis mice after the treatment. (F) Fluorescence images of DHE. (G) Immunofluorescence image of tight junction protein (occludin, ZO-1, and claudin-1). Data were expressed as the mean \pm SD ($n=3$). Statistical analysis was performed using a two-tailed Student's t -test. * $P<0.05$, ** $P<0.01$, and *** $P<0.001$, represented different statistical significances, and ns represents no statistical difference

Modulating gut microbiota by CF@EM

The gut microbiota plays an important role in the regulation of host metabolism, immunity, and intestinal barrier function [35]. After observing the feces of mice, CF@EM was found to improve the fecal status induced by DSS. To verify its regulatory effect on the gut microbiota, we utilized 16S rRNA gene sequencing to analyze the changes. The species accumulation box plot demonstrated sufficient sample size and abundant species richness (Fig. 8A). Species diversity serves as a valuable indicator of the structural and functional characteristics of a community, comprising α -diversity and β -diversity. We analyzed α -diversity through the Shannon index and the Simpson diversity index, and β -diversity through principal component analysis (PCA). The Shannon index described the disorder and uncertainty in the occurrence of individuals among species, while the Simpson diversity

index reflected the probability that two consecutive samples belong to different species. The results showed that the Shannon index and the Simpson diversity index decreased in the DSS group, indicating a decrease in α -diversity. However, treatment with CF@EM increased the reduced α -diversity caused by DSS induction, in line with the control group (Fig. 8B, S9). PCA reflects the differences in multidimensional data as distances in a two-dimensional coordinate plot by downscaling. The closer the distance in the PCA plot, the more similar the community composition of the samples. The PCA results showed that the community composition of the DSS group was different from that of the CF@EM group, suggesting that treatment with CF@EM altered the compositional structure of the gut microbiota (Fig. 8C). Further analysis of species abundance at the phylum and genus level revealed that the abundance of species in the DSS

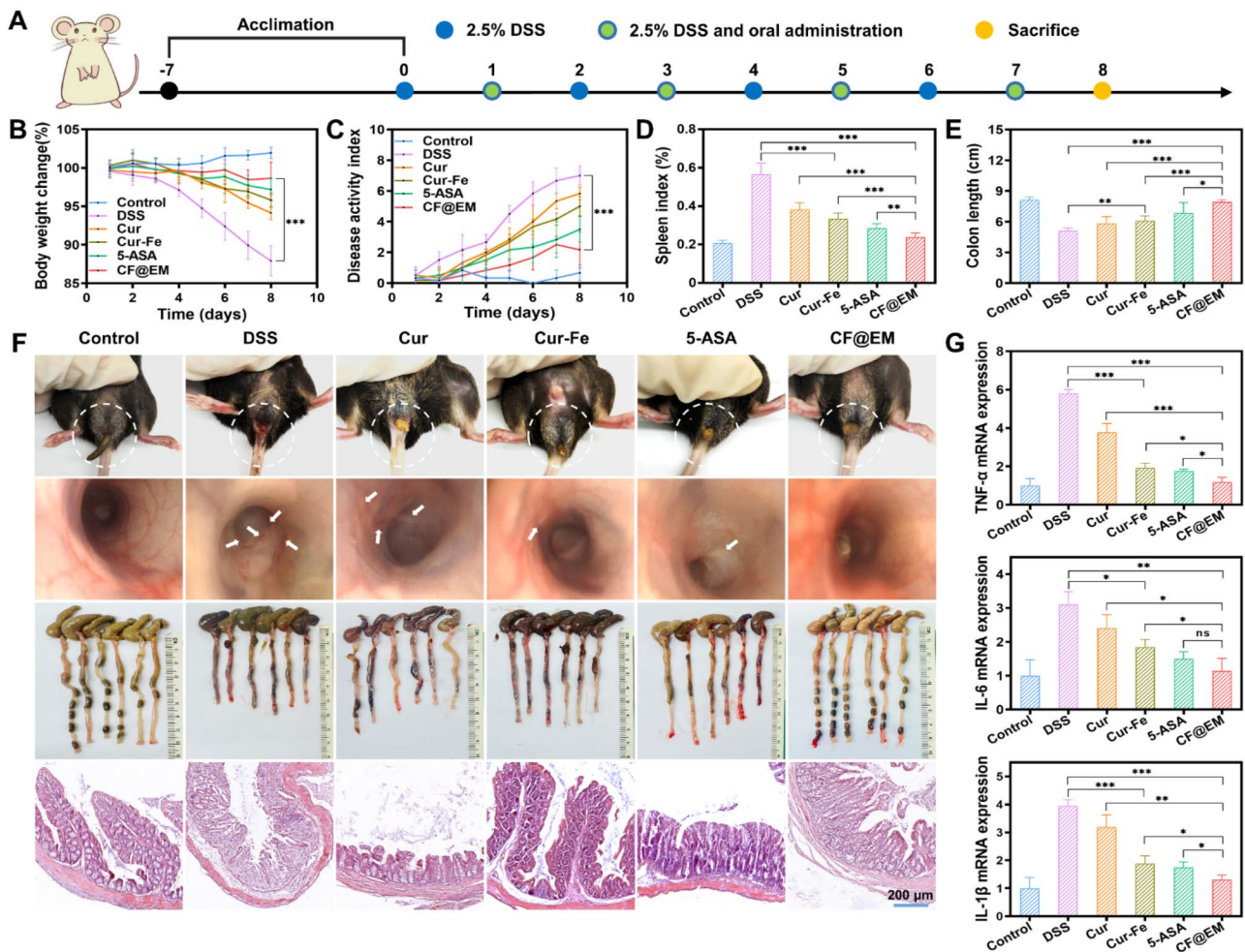


Fig. 7 Preventive effect of CF@EM in DSS-induced colitis. **(A)** Schematic illustration of the establishment and treatment of DSS-induced colitis mice. **(B, C)** Weight change curves **(B)** and DAI curves **(C)** of mice within 8 days. **(D, E)** The spleen index **(D)** and length of the colon **(E)** in different treatment groups. **(F)** Fecal Images, endoscopic images, colon images, and H&E staining of mice in different treatment groups. **(G)** The mRNA expression of TNF- α , IL-6, and IL-1 β in different groups. Data were expressed as the mean \pm SD ($n=6$). Statistical analysis was performed using a two-tailed Student's *t*-test. * $P < 0.05$, ** $P < 0.01$, and *** $P < 0.001$, represented different statistical significances, and ns represents no statistical difference

group was different from that in the CF@EM group (Fig. 8D, E). The abundance of Bacteroidetes is usually closely related to carbohydrate fermentation, nitrogen utilization, and bile acid biotransformation [36]. The abundance of Bacteroidetes was reduced after induction by DSS, and administration of CF@EM increased its abundance in the gut microbiota, with no significant difference in the CF@EM group compared to the control group (Fig. 8F).

Lactobacillus is a group of gram-positive bacteria under the Lactobacillaceae of the Firmicutes, due to the ability of *Lactobacillus* to improve digestion and absorption, catabolize and metabolize bile acids, enhance immunity, and inhibit inflammation [37, 38]. It is now widely studied and used in the food industry. The results showed that the abundance of *Lactobacillus* was significantly reduced in the DSS group, and almost all of them

were inhibited. In contrast, the abundance of *Lactobacillus* in the CF@EM group was restored to the control level (Fig. 8G). The results also showed that the abundance of *Muribaculum* was downregulated by DSS induction, whereas CF@EM significantly increased its abundance and was not significantly different from the control group (Fig. 8H). However, for *Clostridium-sensu-stricto* and *Escherichia-Shigella*, two groups of pathogenic bacteria, CF@EM showed a significant inhibitory effect (Fig. S10) [39–41]. To further explain the observed differences in microbial composition, linear discriminant analysis effect size (LEfSe) was performed. LEfSe was used to identify and interpret high-dimensional biological information, and after identifying significantly different species by intergroup comparisons, the results were analyzed using linear discriminant analysis (LDA) to estimate the magnitude of the effect of each species' abundance on

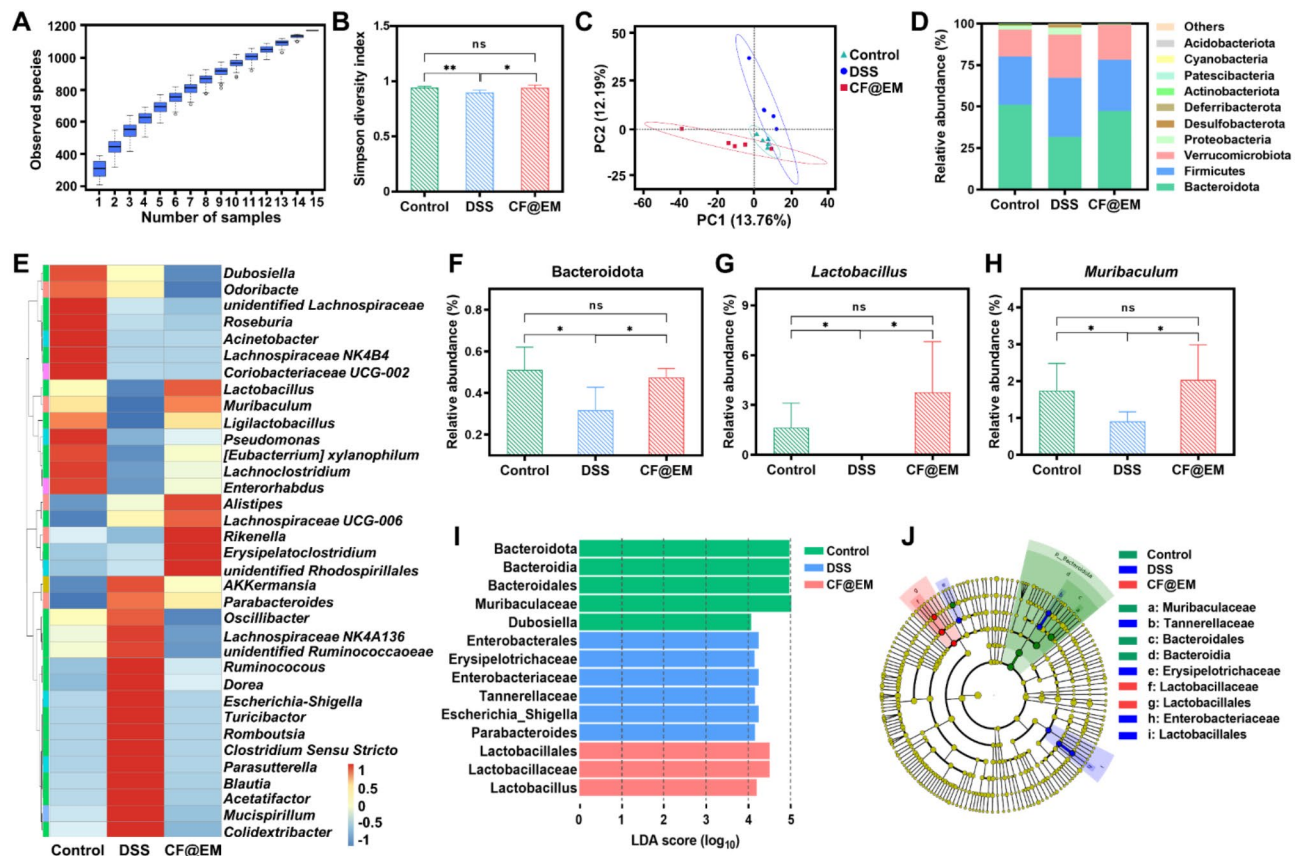


Fig. 8 Regulation of gut microbiota by CF@EM. (A) The species accumulation boxplot. The horizontal coordinate is the number of samples, the vertical coordinate is the number of feature sequences after sampling, and the overall result reflects the rate at which new feature sequences appear under continuous sampling. (B, C) The Simpson diversity index (B) and principal component analysis (C) of the control group, DSS group, and CF@EM group. (D) The abundance at the phylum level. (E) Heatmap of the relative abundance of the 35 most abundant genus-level. (F-H) The abundance of Bacteroidetes (F), *Lactobacillus* (G), and *Muribaculum* (H). (I, J) linear discriminant analysis effect size (LEfSe) and cladogram based on LEfSe analysis. LDA (\log_{10}) > 4 was used as the cutoff value to indicate higher relative abundance in the corresponding group. In a cladogram, circles radiating from the inside out represent taxonomic levels from phylum to genus (or species). Each small circle at a different taxonomic level represents a taxon at that level, and the size of the circle diameter is proportional to the relative abundance size. Species that are not significantly different are uniformly represented in yellow, and green, blue, and red nodes indicate microbial taxa that are significant in the control, DSS, and CF@EM groups. Data were expressed as the mean \pm SD ($n=5$). Statistical analysis was performed using a two-tailed Student's *t*-test. * $P < 0.05$, ** $P < 0.01$, and ns represents no statistical difference

the differential effect. Using LDA (\log_{10}) > 4 as the cut-off value, the results showed that the pathogenic *Escherichia-Shigella* was significantly upregulated in the DSS group, while the beneficial *Lactobacillus* was significantly increased in the CF@EM group (Fig. 8I, J). Taken together, the therapeutic effect of CF@EM on colitis can be partially attributed to the modulation of the gut microbiota, improving bacterial diversity, and transforming the compositional structure of the microbiota to an anti-inflammatory phenotype.

Regulation of gut microbial metabolism by CF@EM

Gut microbiota-host interactions are often mediated by gut microbial metabolites [42]. To further investigate the effect of CF@EM on gut microbial metabolites after regulating gut microbiota composition, we performed fecal metabolomics analysis. The PCA results showed that the

metabolite composition of the DSS group was significantly altered (Fig. 9A), indicating that the metabolites of the gut microbiota were altered by the induction of DSS. By comparing the differences in metabolites between groups, which were plotted as a Venn diagram and volcano plot, it was found that there were a total of 524 differential metabolites in the control group compared with the DSS group, and 216 metabolites were significantly up-regulated and 308 were significantly down-regulated in the DSS group. While there were a total of 529 differential metabolites between the DSS group and the CF@EM group, 315 metabolites were significantly up-regulated and 214 were significantly down-regulated in the CF@EM group (Fig. 9B-D). It was found that the levels of amino acids, fatty acids and conjugates, and indoles and derivatives showed different variations in the DSS group compared to the CF@EM group (Fig. 9E-G). Gut

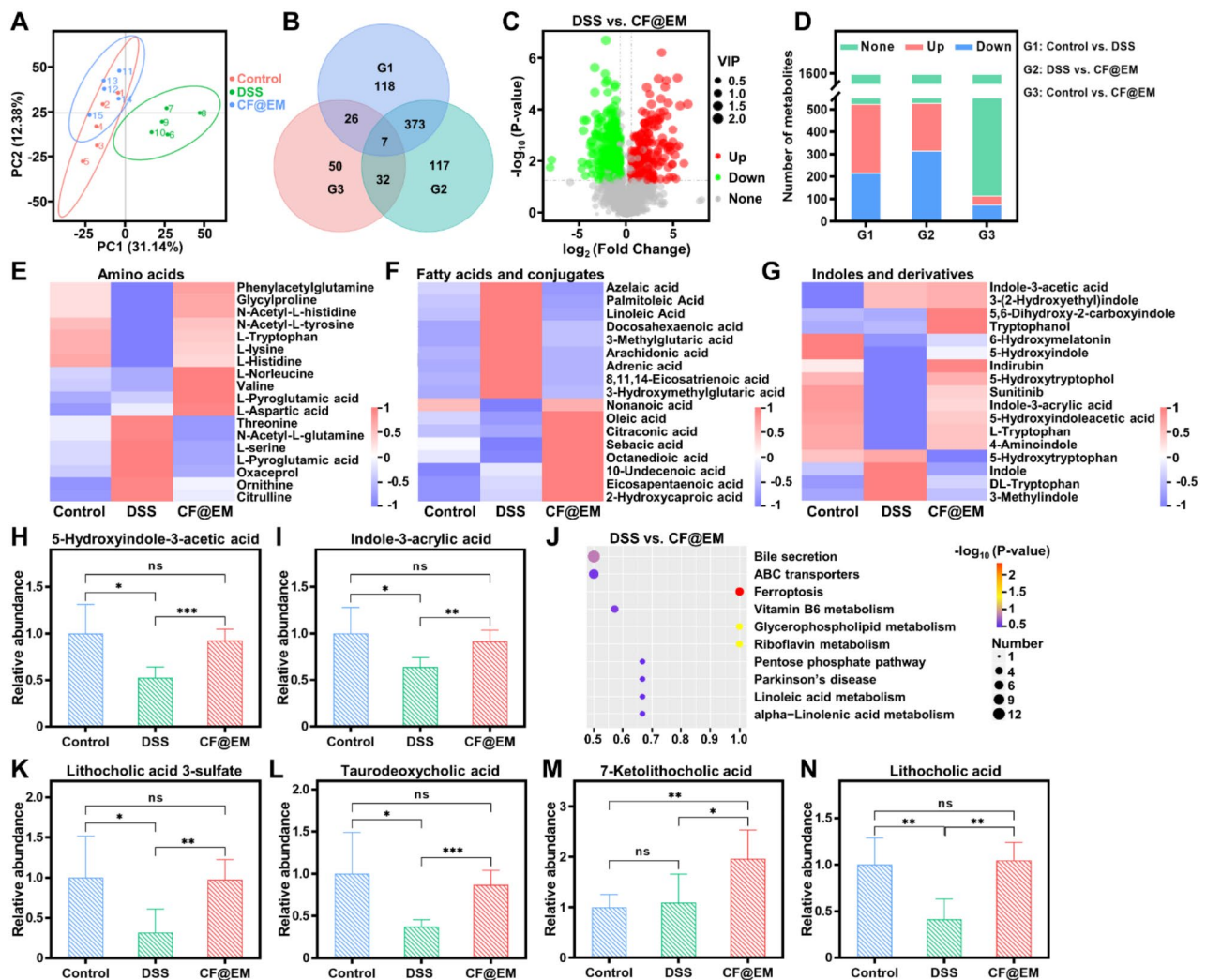


Fig. 9 Regulation of gut microbial metabolites by CF@EM. **(A)** The principal component analysis of the control group, DSS group, and CF@EM group. **(B)** Venn diagram of differential metabolites for between-group comparison. **(C)** Volcano plot of DSS compared with CF@EM. **(D)** Metabolite changes were compared between groups (total metabolites = 1596). **(E)** Relative content of amino acids between control, DSS, and CF@EM groups. **(F)** Relative content of fatty acids and conjugates. **(G–I)** Relative content of indoles and derivatives **(G)**, 5-hydroxyindole-3-acetic acid **(H)**, and indole-3-acrylic acid **(I)**. **(J)** KEGG pathway enrichment analysis of DSS compared with CF@EM. **(K–N)** Relative content of lithocholic acid 3-sulfate **(K)**, taurodeoxycholic acid **(L)**, 7-ketolithocholic acid **(M)**, and lithocholic acid **(N)** between control, DSS and CF@EM groups. Data were expressed as the mean \pm SD ($n=5$). Statistical analysis was performed using a two-tailed Student's *t*-test. * $P < 0.05$, ** $P < 0.01$, and *** $P < 0.001$, represented different statistical significances, and ns represents no statistical difference

microbiota can directly convert aromatic amino acids into indole derivatives, which can maintain intestinal homeostasis by promoting epithelial cell recovery, restoring intestinal barrier function, and modulating immune cell function [43–46]. 5-Hydroxyindole-3-acetic acid and indole-3-acrylic acid were significantly reduced in the DSS group, whereas CF@EM restored them to control levels (Fig. 9H–I). The bile acid pathway was found to be significantly enriched by KEGG enrichment analysis of differential metabolites in the DSS and CF@EM groups (Fig. 9J). Secondary bile acids including lithocholic acid and taurodeoxycholic acid were significantly reduced, which was improved by CF@EM (Fig. 9K–N). Bile acids

and their derivatives have been shown to play an important role in maintaining intestinal homeostasis. Bile acids attenuate intestinal inflammation, modulate intestinal immunity, and improve intestinal barrier function [47, 48], and bile acid receptors mediate the regulation of intestinal inflammation. Bile acid metabolism is significantly dysregulated in IBD, and fecal levels of secondary bile acids are reduced in IBD patients [49, 50]. The above results suggest that the therapeutic effect of CF@EM on colitis may be inextricably linked to bile acid metabolism.

Discussion

Natural polyphenolic compounds are widely used in IBD therapy due to their wide range of anti-inflammatory and ROS scavenging abilities. Encapsulating these compounds in nanomaterials to form polyphenolic nano-preparations is currently the most conventional solution to the problem of low bioavailability [51]. Based on the inherent structural characteristics of curcumin, we have used metal ions to coordinate with it to form a metal-polyphenol structure, which enhances the anti-inflammatory and antioxidant abilities of curcumin and also endows the metal ions with their inherent enzyme-catalytic properties. Numerous studies have shown that iron-based nanozymes have excellent biosafety and multiple enzymatic activities [52]. Coordination of curcumin with iron ions resulted in the formation of Cur-Fe nanozyme, which was found to have excellent multiple free radical scavenging ability in enzyme activity studies.

Due to the complexity of the *in vivo* environment, how to safely and efficiently target and deliver Cur-Fe nanozymes to the site of intestinal inflammation is key to improving the therapeutic efficacy of IBD. Inspired by EcN, the use of EcN membrane-coated nanozymes may be a terrific solution to the problem of intestinal targeting. EcN is a non-pathogenic strain, and due to its surface pili, K5-type capsule, and flagella, it has an excellent ability to colonize the intestine. Meanwhile, it can regulate the gut microbiota, improve the function of the intestinal epithelial barrier, regulate the secretion of immune factors, etc [53]. Due to its outstanding probiotic properties, it has already been used in the treatment of IBD. We have integrated probiotic membranes with bioactive Cur-Fe nanozyme into a system to achieve intestinal colonization and regulation of gut microbiota without interfering with the internal genetic material of the bacteria, which greatly enhances the safety and convenience of probiotic preparations therapy.

The gut microbiota plays a critical role in the pathogenesis of UC by influencing host energy metabolism, regulating immune homeostasis, and maintaining intestinal barrier integrity [54]. Structural perturbations in the composition of the intestinal bacterial community further lead to microbiota dysfunction, thereby exacerbating the intestinal inflammatory response. CF@EM can reverse the decrease in beneficial bacteria and increase in pathogenic bacteria caused by DSS and improve the overall composition of the gut microbiota. Additionally, it can also regulate the levels of gut microbial metabolites and increase the levels of beneficial metabolites such as secondary bile acids, which are reduced in UC patients.

Modulation of host bile acid transport and biosynthesis, along with the composition of the gut microbiota, shapes the bile acid pool [50]. The metabolism of primary bile acids by intestinal bacteria increases the diversity

and overall hydrophobicity of the pool through a variety of modifications such as dehydroxylation, oxidation, and differential isomerization. The bacterial community also regulates bile acid metabolism and transport by influencing signaling pathways mediated by the farnesoid X receptor (FXR) and others involved in lipid and glucose homeostasis, metabolism, and immunomodulatory pathways. Activation of FXR exerts anti-inflammatory effects and has a protective role in chemically induced colitis [55]. Overall, CF@EM may synergize the treatment of UC through multiple pathways, including improving the composition of the gut microbiota, regulating bile acid metabolism, exerting anti-inflammatory effects, and alleviating oxidative stress. This multifaceted approach offers a promising therapeutic avenue for managing UC and its associated symptoms.

However, despite achieving direct, safe, and convenient treatment of UC using a simple oral delivery strategy, the therapeutic effects of CF@EM need to be evaluated in the long term. It is imperative to adequately validate the chronic toxicity and therapeutic efficacy of nanomaterials in chronic colitis models that mimic the characteristics of UC disease. Given the unclear etiology of UC, we have attempted to elaborate on the potential mechanism of action of CF@EM. However, due to the complex pathogenesis and the limitations of animal models, further in-depth exploration of the detailed mechanism of action is warranted. Simultaneously, we expand the application prospects of nanozymes based on clinical enteritis-related diseases.

Conclusion

In summary, inspired by gut microbes, we have successfully synthesized a biomimetic Cur-Fe nanozyme with the ability to inhibit inflammation and restore intestinal homeostasis. The targeted colonization of the probiotic membrane at inflamed intestinal sites has significantly enhanced the cumulative concentration and prolonged the retention time of Cur-Fe nanozyme. Together, these features effectively restore intestinal barrier function and improve the overall intestinal microenvironment, offering a promising therapeutic avenue for gut-related disorders, and novel insights into the development of similar probiotic biomimetic nanozyme drugs.

Supplementary Information

The online version contains supplementary material available at <https://doi.org/10.1186/s12951-024-02802-z>.

Supplementary Material 1

Acknowledgements

We thank Dr. Zijun Ren at the Instrument Analysis Center of Xi'an Jiaotong University for assisting with TEM analysis and Dr. Xiaofei Wang at the

experimental biomedical center of Xi'an Jiaotong University for his kind assistance with the instrument operation and data analysis.

Author contributions

Yuanyuan Zhu: Investigation, Methodology, Data curation, Formal analysis, Software, Validation, Writing-original draft. Xiaoling Huang: Conceptualization, Methodology, Formal analysis, Funding acquisition, Writing-review & editing. Zhichao Deng: Methodology, Investigation. Ting Bai: Investigation, Data curation. Bowen Gao: Investigation, Data curation. Chenxi Xu: Data curation. Junlong Fu: Data curation. Yuanru Zhao: Data curation. Yujie Zhang: Resources, Supervision, Mingxin Zhang: Writing-review & editing, Supervision, Funding acquisition, Project administration. Mingzhen Zhang: Conceptualization, Writing-review & editing, Resources, Supervision, Funding acquisition, Project administration. Mei Yang: Conceptualization, Writing-review & editing, Supervision, Funding acquisition, Project administration. Lina Chen: Conceptualization, Resources, Supervision, Funding acquisition, Project administration.

Funding

This work was supported by the National Natural Science Foundation of China (Nos. 82300598, 82472127), Natural Science Basic Research Program of Shaanxi (2023-JC-ZD-47), the Fundamental Research Funds for the Central Universities, China (No. xtr052023008), and the Young Talent Support Plan of Xi'an Jiaotong University, China (No. YX6J001).

Data availability

No datasets were generated or analysed during the current study.

Declarations

Ethics approval and consent to participate

All work performed on animals was performed following the Guidelines for Care and Use of Laboratory Animals of Xi'an Jiaotong University and approved by the Animal Ethics Committee.

Consent for publication

Not applicable.

Competing interests

The authors declare no competing interests.

Author details

¹Department of Thoracic Surgery, the First Affiliated Hospital of Xi'an Jiaotong University, Xi'an, Shaanxi 710061, China

²Department of Pharmacology, School of Basic Medical Sciences, Xi'an Jiaotong University Health Science Center, Xi'an, Shaanxi 710061, China

³Department of Gastroenterology, People's Hospital of Xinjiang Uygur Autonomous Region, Xinjiang Uygur Autonomous Region, Urumqi 830001, China

⁴School of Basic Medical Sciences, Xi'an Jiaotong University Health Science Center, Xi'an, Shaanxi 710061, China

⁵Department of Cardiovascular Medicine, the First Affiliated Hospital of Xi'an Jiaotong University, Xi'an, Shaanxi 710077, China

⁶Department of Gastroenterology, the First Affiliated Hospital of Xi'an Medical University, Xi'an, Shaanxi 710077, China

⁷Key Laboratory of Environment and Genes Related to Diseases, Xi'an Jiaotong University, Xi'an, Shaanxi 710061, China

Received: 19 June 2024 / Accepted: 22 August 2024

Published online: 06 September 2024

References

- Kobayashi T, Siegmund B, Le Berre C, Wei SC, Ferrante M, Shen B, Bernstein CN, Danese S, Peyrin-Biroulet L, Hibi T. Ulcerative colitis. *Nat Rev Dis Primers*. 2020;6:74.
- Le Berre C, Honap S, Peyrin-Biroulet L. Ulcerative colitis. *Lancet*. 2023;402:571–84.
- Gros B, Kaplan GG. Ulcerative colitis in adults: a review. *JAMA*. 2023;330:951–65.
- Liu JZ, van Sommeren S, Huang H, Ng SC, Alberts R, Takahashi A, Ripke S, Lee JC, Jostins L, Shah T, et al. Association analyses identify 38 susceptibility loci for inflammatory bowel disease and highlight shared genetic risk across populations. *Nat Genet*. 2015;47:979–86.
- Dinallo V, Marafini I, Di Fusco D, Laudisi F, Franze E, Di Grazia A, Figliuzzi MM, Caprioli F, Stolfi C, Monteleone I, Monteleone G. Neutrophil Extracellular traps sustain inflammatory signals in Ulcerative Colitis. *J Crohns Colitis*. 2019;13:772–84.
- Mitsialis V, Wall S, Liu P, Ordovas-Montanes J, Parmet T, Vukovic M, Spencer D, Field M, McCourt C, Toothaker J, et al. Single-cell analyses of Colon and blood reveal distinct Immune Cell signatures of Ulcerative Colitis and Crohn's Disease. *Gastroenterology*. 2020;159:591–e608510.
- Neurath MF. Targeting immune cell circuits and trafficking in inflammatory bowel disease. *Nat Immunol*. 2019;20:970–9.
- Lloyd-Price J, Arze C, Ananthakrishnan AN, Schirmer M, Avila-Pacheco J, Poon TW, Andrews E, Ajami NJ, Bonham KS, Brislawn CJ, et al. Multi-omics of the gut microbial ecosystem in inflammatory bowel diseases. *Nature*. 2019;569:655–62.
- de Vos WM, Tilg H, Van Hul M, Cani PD. Gut microbiome and health: mechanistic insights. *Gut*. 2022;71:1020–32.
- Piovani D, Danese S, Peyrin-Biroulet L, Nikolopoulos GK, Lytras T, Bonovas S. Environmental risk factors for inflammatory Bowel diseases: an Umbrella Review of Meta-analyses. *Gastroenterology*. 2019;157:647–e659644.
- Lopes EW, Chan SSM, Song M, Ludvigsson JF, Hakansson N, Lochhead P, Clark A, Burke KE, Ananthakrishnan AN, Cross AJ, et al. Lifestyle factors for the prevention of inflammatory bowel disease. *Gut*. 2023;72:1093–100.
- Schoefs E, Vermeire S, Ferrante M, Sabino J, Lambrechts T, Avedano L, Haaf I, De Rocchis MS, Broggi A, Sajak-Szczerba M, et al. What are the unmet needs and most relevant Treatment outcomes according to patients with inflammatory bowel disease? A qualitative patient preference study. *J Crohns Colitis*. 2023;17:379–88.
- Stalgis C, Deepak P, Mehandru S, Colombel JF. Rational combination therapy to overcome the Plateau of Drug Efficacy in Inflammatory Bowel Disease. *Gastroenterology*. 2021;161:394–9.
- Luo JH, Shi XS, Li LM, Tan Z, Feng F, Li J, Pang M, Wang XY, He LM. An injectable and self-healing hydrogel with controlled release of curcumin to repair spinal cord injury. *Bioactive Mater*. 2021;6:4816–29.
- Li QR, Lin LT, Zhang C, Zhang HG, Ma Y, Qian HS, Chen XL, Wang XW. The progression of inorganic nanoparticles and natural products for inflammatory bowel disease. *J Nanobiotechnol*. 2024;22:17.
- Tsuda T. Curcumin as a functional food-derived factor: degradation products, metabolites, bioactivity, and future perspectives. *Food Funct*. 2018;9:705–14.
- Geng H, Zhong QZ, Li J, Lin Z, Cui J, Caruso F, Hao J. Metal Ion-Directed Functional Metal-Phenolic materials. *Chem Rev*. 2022;122:11432–73.
- Yuan RYK, Li YQ, Han S, Chen XX, Chen JQ, He J, Gao HW, Yang Y, Yang SL, Yang Y. Fe-Curcumin nanozyme-mediated reactive oxygen species scavenging and anti-inflammation for Acute Lung Injury. *ACS Cent Sci*. 2022;8:10–21.
- Zhang L, Qin ZG, Sun H, Chen X, Dong J, Shen SY, Zheng LM, Gu N, Jiang Q. Nanoenzyme engineered neutrophil-derived exosomes attenuate joint injury in advanced rheumatoid arthritis via regulating inflammatory environment. *Bioactive Mater*. 2022;18:1–14.
- Huang Y, Ren J, Qu X. Nanozymes: classification, Catalytic mechanisms, Activity Regulation, and applications. *Chem Rev*. 2019;119:4357–412.
- Zhang RF, Yan XY, Fan KL. Nanozymes inspired by natural enzymes. *Acc Mater Res*. 2021;2:534–47.
- Fu W, Xu L, Chen Z, Kan L, Ma Y, Qian H, Wang W. Recent advances on emerging nanomaterials for diagnosis and treatment of inflammatory bowel disease. *J Control Release*. 2023;363:149–79.
- Singh N, Sherin GR, Mugesh G. Antioxidant and prooxidant nanozymes: from Cellular Redox Regulation to Next-Generation therapeutics. *Angew Chem Int Ed Engl*. 2023;62:e202301232.
- McCallum G, Tropini C. The gut microbiota and its biogeography. *Nat Rev Microbiol*. 2023;22:105–18.
- Wan Y, Yang L, Jiang S, Qian D, Duan J. Excessive apoptosis in Ulcerative Colitis: Crosstalk between apoptosis, ROS, ER stress, and intestinal homeostasis. *Inflamm Bowel Dis*. 2022;28:639–48.
- Bourgonje AR, Kloska D, Grochot-Przeczek A, Feelisch M, Cuadrado A, van Goor H. Personalized redox medicine in inflammatory bowel diseases: an emerging role for HIF-1alpha and NRF2 as therapeutic targets. *Redox Biol*. 2023;60:102603.
- Jin T, Lu HY, Zhou Q, Chen DF, Zeng YY, Shi JY, Zhang YM, Wang XW, Shen XK, Cai XJ. H2S-Releasing versatile Montmorillonite Nanof ormulation Trilogically

- renovates the Gut Microenvironment for Inflammatory Bowel Disease Modulation. *Adv Sci.* 2024;11:2308092.
28. Haifer C, Paramsothy S, Kaakoush NO, Saikal A, Ghaly S, Yang T, Luu LDW, Borody TJ, Leong RW. Lyophilised oral faecal microbiota transplantation for ulcerative colitis (LOTUS): a randomised, double-blind, placebo-controlled trial. *Lancet Gastroenterol Hepatol.* 2022;7:141–51.
 29. Sorbara MT, Pamer EG. Microbiome-based therapeutics. *Nat Rev Microbiol.* 2022;20:365–80.
 30. Suez J, Zmora N, Segal E, Elinav E. The pros, cons, and many unknowns of probiotics. *Nat Med.* 2019;25:716–29.
 31. Xu JQ, Xu JC, Shi TF, Zhang YL, Chen FM, Yang C, Guo XJ, Liu GN, Shao D, Leong KW, Nie GJ. Probiotic-inspired nanomedicine restores intestinal homeostasis in colitis by regulating Redox Balance, Immune responses, and the gut Microbiome. *Adv Mater.* 2023;35:2207890.
 32. Hegarty LM, Jones GR, Bain CC. Macrophages in intestinal homeostasis and inflammatory bowel disease. *Nat Rev Gastroenterol Hepatol.* 2023;20:538–53.
 33. Horowitz A, Chanez-Paredes SD, Haest X, Turner JR. Paracellular permeability and tight junction regulation in gut health and disease. *Nat Rev Gastroenterol Hepatol.* 2023;20:417–32.
 34. Otani T, Furuse M. Tight Junction structure and function revisited. *Trends Cell Biol.* 2020;30:805–17.
 35. Ni J, Wu GD, Albenberg L, Tomov VT. Gut microbiota and IBD: causation or correlation? *Nat Rev Gastroenterol Hepatol.* 2017;14:573–84.
 36. Gibiino G, Lopetuso LR, Scaldaferri F, Rizzatti G, Binda C, Gasbarrini A. Exploring Bacteroidetes: metabolic key points and immunological tricks of our gut commensals. *Dig Liver Dis.* 2018;50:635–9.
 37. Heeney DD, Gareau MG, Marco ML. Intestinal *Lactobacillus* in health and disease, a driver or just along for the ride? *Curr Opin Biotechnol.* 2018;49:140–7.
 38. Goldstein EJ, Tyrrell KL, Citron DM. *Lactobacillus* species: taxonomic complexity and controversial susceptibilities. *Clin Infect Dis.* 2015;60(Suppl 2):S98–107.
 39. Udaondo Z, Duque E, Ramos JL. The pangenome of the genus *Clostridium*. *Environ Microbiol.* 2017;19:2588–603.
 40. He XX, Li YH, Yan PG, Meng XC, Chen CY, Li KM, Li JN. Relationship between clinical features and intestinal microbiota in Chinese patients with ulcerative colitis. *World J Gastroenterol.* 2021;27:4722–37.
 41. Zhang Z, Taylor L, Shommu N, Ghosh S, Reimer R, Panaccione R, Kaur S, Hyun JE, Cai C, Deehan EC, et al. A Diversified Dietary Pattern is Associated with a balanced gut Microbial Composition of Faecalibacterium and Escherichia/Shigella in patients with Crohn's Disease in Remission. *J Crohns Colitis.* 2020;14:1547–57.
 42. Krautkramer KA, Fan J, Backhed F. Gut microbial metabolites as multi-kingdom intermediates. *Nat Rev Microbiol.* 2021;19:77–94.
 43. Li X, Zhang B, Hu Y, Zhao Y. New insights into gut-Bacteria-derived Indole and its derivatives in Intestinal and Liver diseases. *Front Pharmacol.* 2021;12:769501.
 44. Agus A, Planchais J, Sokol H. Gut microbiota regulation of Tryptophan Metabolism in Health and Disease. *Cell Host Microbe.* 2018;23:716–24.
 45. Li J, Zhang L, Wu T, Li Y, Zhou X, Ruan Z. Indole-3-propionic acid improved the intestinal barrier by enhancing epithelial barrier and mucus barrier. *J Agric Food Chem.* 2021;69:1487–95.
 46. Lavelle A, Sokol H. Gut microbiota-derived metabolites as key actors in inflammatory bowel disease. *Nat Reviews Gastroenterol Hepatol.* 2020;17:223–37.
 47. Hang S, Paik D, Yao L, Kim E, Trinath J, Lu J, Ha S, Nelson BN, Kelly SP, Wu L, et al. Bile acid metabolites control T(H)17 and T(reg) cell differentiation. *Nature.* 2019;576:143–8.
 48. Song X, Sun X, Oh SF, Wu M, Zhang Y, Zheng W, Geva-Zatorsky N, Jupp R, Mathis D, Benoist C, Kasper DL. Microbial bile acid metabolites modulate gut RORgamma(+) regulatory T cell homeostasis. *Nature.* 2020;577:410–5.
 49. Nicolas GR, Chang PV. Deciphering the Chemical lexicon of host-gut microbiota interactions. *Trends Pharmacol Sci.* 2019;40:430–45.
 50. Collins SL, Stine JG, Bisanz JE, Okafor CD, Patterson AD. Bile acids and the gut microbiota: metabolic interactions and impacts on disease. *Nat Rev Microbiol.* 2023;21:236–47.
 51. Wang H, Wang CP, Zou Y, Hu JJ, Li YW, Cheng YY. Natural polyphenols in drug delivery systems: current status and future challenges. *Giant.* 2020;3:100022.
 52. Zhu R, Cai M, Fu T, Yin D, Peng H, Liao S, Du Y, Kong J, Ni J, Yin X. Fe-Based Metal Organic frameworks (Fe-MOFs) for bio-related applications. *Pharmaceutics.* 2023;15:1599.
 53. Behrouzi A, Mazaheri H, Falsafi S, Tavassol ZH, Moshiri A, Siadat SD. Intestinal effect of the probiotic *Escherichia coli* strain Nissle 1917 and its OMV. *J Diabetes Metab Disord.* 2020;19:597–604.
 54. Franzosa EA, Sirota-Madi A, Avila-Pacheco J, Fornelos N, Haiser HJ, Reinker S, Vatanen T, Hall AB, Mallick H, McIver LJ, et al. Gut microbiome structure and metabolic activity in inflammatory bowel disease. *Nat Microbiol.* 2019;4:293–305.
 55. Wahlstrom A, Sayin SI, Marschall HU, Backhed F. Intestinal crosstalk between bile acids and microbiota and its impact on host metabolism. *Cell Metab.* 2016;24:41–50.

Publisher's note

Springer Nature remains neutral with regard to jurisdictional claims in published maps and institutional affiliations.